

Dual-Channel Tensor Neural Networks: Finite-Sample Theory and Conformal Structure Selection

Elynn Chen^{#*} Jiayu Li[◇] Zheshi Zheng[♭] Jian Pei[†]
^{#,◇}New York University [♭] University of Michigan [†] Duke University

May 20, 2026

Abstract

Tensor-valued data arise naturally in neuroimaging, genomics, climate science, and spatiotemporal networks, where multilinear dependencies across modes carry information that is destroyed under vectorization. Existing approaches either impose a single low-rank structure, which can miss localized signal, or treat the tensor as a long vector, which discards its multiway geometry. We propose a *Dual-Channel Tensor Neural Network* (DC-TNN) that decomposes each tensor input into a low-rank core and a sparse refinement, and processes the two components through coupled neural channels. The framework is structure-agnostic and accommodates CP, Tucker, and tensor-train cores within a single architecture. For estimation, we establish non-asymptotic risk bounds for the DC-TNN estimator that decompose into network approximation, core estimation, and refinement-selection terms, and show that the effective dimension is determined jointly by the core rank and refinement sparsity rather than by the ambient tensor size. For inference, we develop a *structure-aware conformal ROC* procedure that calibrates within the core-refinement latent space and produces ROC and AUC confidence bands with finite-sample, distribution-free coverage. Building on this, we propose a *conformal structure selector* that, to our knowledge, is the *first distribution-free procedure* for choosing among candidate tensor decompositions with finite-sample validity. Simulations and an analysis of a protein dataset demonstrate competitive predictive accuracy, reliable uncertainty quantification, and consistent recovery of the tensor structure.

Keywords: high-dimensional tensor regression; ReLU networks; conformal prediction; ROC and AUC inference; tensor decomposition selection.

*Correspondence to E. Chen (E-mail: elynn.chen@stern.nyu.edu) and J. Pei (E-mail: j.pei@duke.edu).

1 Introduction

Modern machine learning applications increasingly involve *high-dimensional structured data* that naturally arise as tensors, including multi-modal biomedical measurements, spatiotemporal signals, and graph-structured representations (Chen, Yun, Chen & Yao 2020, Chen & Chen 2022, Wen et al. 2024, Kong et al. 2025). Unlike vectorized inputs, tensor data preserve rich *multiway dependencies across modes*, which are critical for capturing complex interactions and improving predictive performance (Wen et al. 2024, Kong et al. 2025, Wu, Mo, Chen & Chen 2025). A central challenge in learning from such data is that their underlying structure is often *heterogeneous*: global patterns governed by low-dimensional latent factors coexist with *localized, irregular, or sparse variations* that carry important predictive signals. Developing models that can effectively capture both types of structure remains a fundamental problem in modern data mining and machine learning.

Existing approaches typically address high-dimensional tensor data by imposing *either low-rank structure or sparsity*, but each paradigm is fundamentally limited in heterogeneous settings. Low-rank models, including CP, Tucker, and tensor-train representations, are effective at summarizing global multilinear dependencies, yet they often suffer from *representation bias* when localized signal components are not aligned with the assumed low-rank subspace. Conversely, sparse or high-dimensional nonparametric models provide flexibility to capture localized effects, but they largely ignore the underlying tensor structure and therefore incur an *inflated effective dimension*, leading to reduced statistical and computational efficiency. As a result, neither paradigm alone is sufficient for modeling real-world tensor data that exhibit both global structure and local variability (Chen et al. 2026, Chen, Han, Li & Xu 2025).

These limitations suggest that the key challenge is not merely the selection of a specific

tensor decomposition (e.g., CP versus Tucker), but rather a broader problem of *learning under structural uncertainty*. In practice, the true data-generating mechanism may not conform to a single homogeneous structure; instead, it often lies in a richer class that combines *low-rank global components with sparse, localized refinements*. This perspective reframes tensor learning as a *model class selection problem*, where the goal is to identify and learn an appropriate hybrid structure that balances global regularity and local flexibility. An effective framework should therefore avoid committing to a single structural assumption a priori, and instead enable adaptive integration of multiple structural components within a unified model.

To address this challenge, we propose a *dual-channel neural architecture* for learning predictive functions over tensor inputs with heterogeneous structure. The key idea is to decompose the input into two complementary components: a *low-rank core* capturing dominant multilinear patterns, and a *refinement component* encoding localized deviations. These components are processed through parallel network channels and are coupled via *cross-channel interactions*, enabling the model to jointly exploit global and local information (Wen et al. 2024, Kong et al. 2025, Wen et al. 2025). The resulting framework provides a flexible yet structured inductive bias that generalizes both pure low-rank tensor models and high-dimensional models, allowing the model to adapt to different structural regimes in the data.

Beyond the architectural design, the proposed framework introduces a new *structured function class* that bridges low-rank tensor models and high-dimensional sparse models (Chen et al. 2026, Chen, Han & Li 2024b, 2025). By jointly modeling a low-dimensional global component and a sparse refinement component, the framework effectively interpolates between these two regimes, capturing a wider range of data-generating mechanisms. This perspective provides a unified view of tensor modeling and enables a principled analysis

of how structural assumptions influence generalization, highlighting the trade-offs between approximation accuracy, structural bias, and model complexity.

In addition to predictive modeling, we incorporate *uncertainty quantification* to provide more reliable evaluation and decision-making (Wu et al. 2024, Wu, Yang, Chen, Chen & Zheng 2025). Standard conformal prediction methods, when applied to high-dimensional tensor data, typically ignore the underlying structure and treat inputs as unstructured vectors, leading to overly conservative and less informative uncertainty estimates. In contrast, we develop a structure-aware conformal inference procedure that operates on the proposed model, yielding *sharper and more informative confidence regions* for performance metrics such as ROC curves and AUC (Wu, Yang, Chen, Chen & Zheng 2025), while maintaining distribution-free validity.

A further innovation of this work is a principled approach to *model selection under structural uncertainty*. In practice, choosing among candidate tensor structures (e.g., CP, Tucker) is typically done using heuristic validation procedures that do not account for uncertainty arising from finite samples or model fitting. We address this limitation by developing a statistically grounded selection procedure that compares competing models through their predictive performance while incorporating uncertainty. This allows us to determine whether one structure is significantly better than another, or whether multiple structures are statistically indistinguishable.

The main contributions of this paper are summarized as follows:

- *Structured Modeling Framework*. We propose a dual-channel neural architecture that learns global-local representations for tensor data by jointly modeling low-rank structure and sparse refinements within a unified framework.
- *Unified Modeling Perspective*. We introduce a new function class that bridges low-

rank tensor models and high-dimensional sparse models, providing a principled view of representation learning under heterogeneous structural assumptions.

- *Uncertainty Quantification.* We develop a structure-aware conformal inference method that produces sharper and more informative uncertainty estimates for predictive performance.
- *Model Selection under Structural Uncertainty.* We propose a statistically grounded procedure for selecting among competing tensor structures, addressing a key gap in existing methods.
- *Theoretical Guarantees.* We establish non-asymptotic generalization bounds and show that the proposed framework achieves optimal rates while explicitly characterizing the trade-offs between approximation accuracy, structural bias, and model complexity in hybrid representation learning.

We validate the proposed approach through extensive experiments on synthetic and real-world datasets. The results demonstrate improved predictive performance in heterogeneous settings, effective recovery of underlying structural patterns, and reliable uncertainty quantification and model selection. These findings highlight the practical advantages of combining structured inductive bias with flexible predictive modeling in tensor-based learning problems.

1.1 Related Work and Our Distinctions

For clarity we group related work into three threads and state our distinctions explicitly.

Tensor regression with low-rank, sparse, or hybrid structure. The foundational tensor regression literature establishes CP- and Tucker-based generalized linear models

(Zhou et al. 2013, Li et al. 2018, Chen, Xia, Cai & Fan 2024, Xu et al. 2025), tensor-train regression (Si et al. 2022), tensor-response and tensor-on-tensor regression (Sun et al. 2017, Li & Zhang 2017, Lock 2018, Raskutti et al. 2019), Bayesian tensor regression (Guhaniyogi et al. 2017), and provable sparse tensor decomposition (Sun et al. 2017). A related body of work develops matrix- and tensor-variate factor models that exploit multilinear low-rank structure for dimension reduction and prediction (Chen, Tsay & Chen 2020, Chen & Fan 2023, Liu & Chen 2022, 2019, Chen, Chen, Bolivar & Chen 2024), as well as factor-augmented regression that incorporates latent factors as predictors (Chen et al. 2026). The hybrid linear line, including Tucker-with-sparsity (Ahmed et al. 2020), boosted sparse CP (He et al. 2018), cubic sketching for sparse-and-low-rank tensors (Hao et al. 2020), and the generalized low-rank-plus-sparse estimator of (Cai et al. 2023), considers both low-rank and sparse components. Tensor classification and discriminant analysis under CP and Tucker low-rank structures (Chen, Han & Li 2024a,b, 2025, Liu et al. 2025) further illustrate the value of exploiting tensor structure in supervised learning. The non-asymptotic theory of generalized tensor estimation is developed in (Han et al. 2022), with recent inference advances for low-rank tensor models in (Xu et al. 2025).

We depart from this body of work in two respects. First, where these methods impose low-rank-plus-sparse structure on a *linear* coefficient tensor, we model the regression function as a *nonlinear* map on the latent representation $(\mathcal{C}, \mathcal{V}_{\mathcal{J}})$, producing a strictly richer function class. Second, we provide finite-sample distribution-free inference and a structure-selection procedure, neither of which exists for the linear estimators.

Neural networks for tensor inputs and for nonparametric regression. On the architectural side, weight-tensorization methods (Novikov et al. 2015, Kossaifi et al. 2020) reduce parameter counts but do not model input structure, do not separate global from local components, and do not provide non-asymptotic statistical guarantees. Tensor-contraction

and tensor-augmented architectures (Wen et al. 2024, Wu et al. 2024, Wu, Mo, Chen & Chen 2025, Wu, Yang, Chen, Chen & Zheng 2025, Kong et al. 2025, Wen et al. 2025) preserve multilinear structure in activations but operate with a single, fixed structural assumption. On the theoretical side, our analysis builds on the analysis for deep ReLU networks under Hölder smoothness (Schmidt-Hieber 2020, Bauer & Kohler 2019, Kohler & Langer 2021), revised here in the tensor-input setting and combined with tensor-factor-model error propagation (Zhang & Xia 2018, Chen, Han & Li 2024a).

The closest methodological predecessor is FAST-NN (Fan & Gu 2023), which establishes the latent-factor-plus-sparse-idiosyncratic paradigm for deep ReLU networks with vector covariates; our framework lifts that paradigm to tensor covariates and substantially extends it through structure-aware inference and tensor structure selection.

Conformal inference for classification and ROC curves. Split conformal prediction supplies distribution-free intervals and prediction sets (Vovk et al. 2005, Shafer & Vovk 2008, Lei et al. 2018), with extensions to heteroscedastic regression (Romano et al. 2019) and localized calibration (Guan 2023). For classification, recent work develops conformal ROC and AUC inference (Zheng et al. 2024, 2025) and adapts conformal ideas to tensorized graph models (Wu et al. 2024, Wu, Yang, Chen, Chen & Zheng 2025). Applied to tensor inputs, these methods calibrate in the ambient space and yield conservative bands. Our procedure calibrates in the DC-TNN’s latent core-refinement representation, producing sharper bands while retaining distribution-free coverage, and extends to the difference-ROC setting that underlies our structure selector. To our best knowledge, this is the first prediction-based test for low-rank tensor structure selection with finite-sample validity.

Organization. Section 2 formalizes the core-refinement model and the DC-TNN architecture. Section 3 details the two-stage training procedure. Section 4 develops the finite-sample theory. Section 5 develops the structure-aware conformal inference procedure. Sec-

tion 6 introduces the conformal structure selector. Sections 7 and 8 report simulation and real-data results on the DD protein benchmark. Section 9 concludes. Proofs, the end-to-end training procedure, the tensor-train variant, and additional experiments are deferred to the supplement.

2 Structured Modeling of Heterogeneous Tensor Data

We consider learning predictive models from *high-dimensional tensor inputs*, where each observation is a multiway array $\mathcal{X} \in \mathbb{R}^{D_1 \times \dots \times D_M}$. A key challenge is that real-world tensors often exhibit *heterogeneous structure*, where global low-rank patterns coexist with *localized and irregular variations* that are critical for prediction.

2.1 Structured Feature Transformation

To address this challenge, we consider a decomposition of the form

$$\mathcal{X} = \mathcal{S}(\mathcal{C}) + \mathcal{V}, \tag{1}$$

where $\mathcal{C} \in \mathbb{R}^{R_1 \times \dots \times R_M}$ is a latent core tensor with $R_m \ll D_m$, and $\mathcal{S} : \mathbb{R}^{R_1 \times \dots \times R_M} \rightarrow \mathbb{R}^{D_1 \times \dots \times D_M}$ is a multilinear map that expands \mathcal{C} into the ambient tensor space. The term $\mathcal{S}(\mathcal{C})$ represents a *global low-rank component*, encoding dominant multilinear interactions, while \mathcal{V} captures *localized or idiosyncratic variations* not explained by the global structure.

Importantly, this decomposition is not imposed as a generative model, but defines a *structured feature transformation*: $\mathcal{X} \mapsto (\mathcal{C}, \mathcal{V})$. Since \mathcal{V} captures localized and irregular deviations from the global structure, it is expected to be sparse, only a small subset of its entries carry predictive information. This motivates restricting to local features $\mathcal{V}_{\mathcal{J}}$, the entries of \mathcal{V} indexed by \mathcal{J} , reducing the transformation to $\mathcal{X} \mapsto (\mathcal{C}, \mathcal{V}_{\mathcal{J}})$. The index set \mathcal{J} is determined by a sparsity-constrained selection procedure detailed in Section 3.

This transformation serves as a form of *structured inductive bias*, rather than a constraint on the predictive model itself. The predictive function is then modeled as a *nonlinear mapping over* $(\mathcal{C}, \mathcal{V}_{\mathcal{J}})$, integrating *low-rank global structure with sparse local flexibility*, and effectively reducing complexity compared to operating directly in the ambient tensor space.

2.2 Dual-Channel Neural Architecture

Building on the structured feature transformation, we propose a *dual-channel neural architecture* that jointly models global and local components by processing \mathcal{C} and $\mathcal{V}_{\mathcal{J}}$ through *separate but interacting channels*. The *core channel* \mathcal{H}_c operates on the low-dimensional core tensor \mathcal{C} , learning representations that capture global multilinear dependencies. In parallel, the *refinement channel* \mathcal{H}_u processes $\mathcal{U} \in \mathbb{R}^{K_1 \times \dots \times K_M}$, a dense tensor induced by \mathcal{V} , storing the selected entries of the local component \mathcal{V} indexed by \mathcal{J} , with dimensions K_1, \dots, K_M chosen such that $\prod_{m=1}^M K_m \geq |\mathcal{J}|$ and approximately balanced ($K_1 \asymp \dots \asymp K_M$), ensuring sufficient capacity to represent all active refinement locations. The two channels are coupled through *cross-channel interactions*, allowing information to flow between global and local representations at each layer, enabling the model to adaptively combine structured and flexible components.

We initialize $\mathcal{H}_c^{(0)} = \mathcal{C}$ and $\mathcal{H}_u^{(0)} = \mathcal{U}$. At each layer ℓ , let $\mathcal{H}_c^{(\ell)} \in \mathbb{R}^{R_1^{(\ell)} \times \dots \times R_M^{(\ell)}}$ and $\mathcal{H}_u^{(\ell)} \in \mathbb{R}^{K_1^{(\ell)} \times \dots \times K_M^{(\ell)}}$ denote the hidden states of the core and refinement channels. The layerwise updates are given by

$$\begin{aligned} \text{Core } (\mathcal{C}) \text{ channel: } \mathcal{H}_c^{(\ell+1)} &:= \alpha_c (\mathcal{W}_{cc}^{(\ell)} \bullet \mathcal{H}_c^{(\ell)} + \mathcal{W}_{cu}^{(\ell)} \bullet \mathcal{H}_u^{(\ell)} + \mathcal{B}_c^{(\ell)}), \\ \text{Refinement } (\mathcal{U}) \text{ channel: } \mathcal{H}_u^{(\ell+1)} &:= \alpha_u (\mathcal{W}_{uc}^{(\ell)} \bullet \mathcal{H}_c^{(\ell)} + \mathcal{W}_{uu}^{(\ell)} \bullet \mathcal{H}_u^{(\ell)} + \mathcal{B}_u^{(\ell)}), \end{aligned} \tag{2}$$

where α_c, α_u are nonlinear activation functions applied elementwise, and \bullet denotes tensor contraction along matching modes. The weight tensors $(\mathcal{W}_{cc}^{(\ell)}, \mathcal{W}_{uu}^{(\ell)})$ learn structure within each channel, while $(\mathcal{W}_{cu}^{(\ell)}, \mathcal{W}_{uc}^{(\ell)})$ model the interactions between the core and refinement

representations. The bias tensors $\mathcal{B}_c^{(\ell)} \in \mathbb{R}^{\times_{m=1}^M R_m^{(\ell+1)}}$ and $\mathcal{B}_u^{(\ell)} \in \mathbb{R}^{\times_{m=1}^M K_m^{(\ell+1)}}$ account for affine shifts.

Denote by $\mathcal{T}^{(\ell+1)}(\cdot, \cdot)$ the parallel update operator in (2), which maps $(\mathcal{H}_c^{(\ell)}, \mathcal{H}_u^{(\ell)}) \rightarrow (\mathcal{H}_c^{(\ell+1)}, \mathcal{H}_u^{(\ell+1)})$, $\ell = 0, \dots, L-1$. After L hidden layers, we apply a final linear operator

$$\mathcal{T}^{(L+1)}(\mathcal{H}_c^{(L)}, \mathcal{H}_u^{(L)}) = \mathcal{W}_c^{(L)} \bullet \mathcal{H}_c^{(L)} + \mathcal{W}_u^{(L)} \bullet \mathcal{H}_u^{(L)} + \mathcal{B}^{(L)},$$

with $\mathcal{W}_c^{(L)} \in \mathbb{R}^{d^{(L+1)} \times \times_{m=1}^M R_m^{(L)}}$, $\mathcal{W}_u^{(L)} \in \mathbb{R}^{d^{(L+1)} \times \times_{m=1}^M K_m^{(L)}}$, and the bias $\mathcal{B}^{(L)} \in \mathbb{R}^{d^{(L+1)}}$. The resulting output is a $d^{(L+1)}$ -dimensional vector (with $d^{(L+1)} = 1$ for scalar regression, and $d^{(L+1)} = K-1$ for K -category classification). Thus, the dual-channel tensor neural network defines the mapping

$$f(\mathcal{C}, \mathcal{U}) = \alpha(\mathcal{T}^{(L+1)} \circ \mathcal{T}^{(L)} \circ \dots \circ \mathcal{T}^{(1)}(\mathcal{C}, \mathcal{U})), \quad (3)$$

where α denotes the link function (identity for regression, logistic or softmax for classification). The operator in (3) defines a class of dual-channel tensor neural networks, formalized in Definition 1 and illustrated in Figure 1.

Definition 1 (Dual-Channel Deep ReLU Tensor Network).

Let $\mathbf{d}^{(\ell)} = (R_1^{(\ell)}, \dots, R_M^{(\ell)}, K_1^{(\ell)}, \dots, K_M^{(\ell)})$ denote a $2M$ -dimensional width vector at layer ℓ , where the first M entries specify the widths of the core channel and the remaining M entries specify those of the refinement channel. Define the width tuple $\mathbf{d} = (\mathbf{d}^{(1)}, \dots, \mathbf{d}^{(L)}, d^{(L+1)})$, where $d^{(L+1)} \in \mathbb{N}$ is the output width of the final layer.

For any depth $L \in \mathbb{N}$, width tuple \mathbf{d} , truncation level $V \in \mathbb{R}^+ \cup \{\infty\}$, and weight bound $B \in \mathbb{R}^+$, the class of truncated dual-channel deep ReLU tensor networks is defined as

$$\mathcal{F}(L, \mathbf{d}, V, B) = \{\bar{f}(\mathcal{C}, \mathcal{U}) = \mathcal{T}_V(f(\mathcal{C}, \mathcal{U}))\},$$

where $f(\mathcal{C}, \mathcal{U})$ is the DC-TNN mapping defined in (3) with parameters satisfying

$$\max_{1 \leq \ell \leq L} \{ \|\mathcal{W}_{cc}^{(\ell)}\|_{\max}, \|\mathcal{W}_{cu}^{(\ell)}\|_{\max}, \|\mathcal{W}_{uu}^{(\ell)}\|_{\max}, \|\mathcal{W}_{uc}^{(\ell)}\|_{\max}, \|\mathcal{B}_u^{(\ell)}\|_{\max}, \|\mathcal{B}_c^{(\ell)}\|_{\max} \} \leq B,$$

and the output-layer parameters satisfy $\|\mathcal{W}_c^{(L)}\|_{\max}, \|\mathcal{W}_u^{(L)}\|_{\max}, \|\mathcal{B}^{(L)}\|_{\max} \leq B$. Here, $\mathcal{T}_V(\cdot)$ denotes elementwise truncation at level V : $[\mathcal{T}_V(z)] = \text{sgn}(z)(|z| \wedge V)$ applied to each coordinate of the output. For brevity, when the width tuple is of the form $\mathbf{d} = (\mathbf{d}_{in}, \mathbf{w}, \dots, \mathbf{w}, d_{out})$, we write $\mathcal{F}(L, \mathbf{d}_{in}, d_{out}, \mathbf{w}, V, B)$.

Remark 1. The architecture in Definition 1 encompasses several important special cases in tensor learning. When all cross- and refinement-channel weights vanish, i.e., $\mathcal{W}_{uc}^{(\ell)} = \mathcal{W}_{cu}^{(\ell)} = \mathcal{W}_{uu}^{(\ell)} = 0$ for all ℓ , the network reduces to a tensor neural network operating solely on \mathcal{C} , corresponding to a purely low-rank model. Conversely, when all core-related weights vanish, i.e., $\mathcal{W}_{uc}^{(\ell)} = \mathcal{W}_{cu}^{(\ell)} = \mathcal{W}_{cc}^{(\ell)} = 0$, the network operates solely on \mathcal{U} , which can be viewed as a sparsity-constrained model. More generally, the dual-channel formulation unifies these two complementary mechanisms: the core channel captures structured multilinear interactions through a low-dimensional latent tensor, while the refinement channel provides localized, sparsity-constrained flexibility. Together, they enable richer representations than either mechanism alone.

2.3 Model Instantiations and Structural Variants

The framework in (1) can be instantiated using different choices of the signal map $\mathcal{S}(\cdot)$, including Tucker, and CP decompositions, each inducing a distinct structural bias on the global component \mathcal{C} . Since in practice, the appropriate structure is often unknown and depends on the underlying data, we address *data-driven selection among candidate structures* through a principled model selection procedure developed in Section 6.

Tucker-Core Adaptation. Each tensor covariate $\mathcal{X}_i \in \mathbb{R}^{\times_{m=1}^M D_m}$ is decomposed as

$$\mathcal{X}_i = S(\mathcal{C}_i) + \mathcal{V}_i = \mathcal{C}_i \times_{m=1}^M \mathbf{A}_m + \mathcal{V}_i, \quad i \in [n], \quad (4)$$

where $\mathcal{C}_i \in \mathbb{R}^{\times_{m=1}^M R_m}$ is the latent Tucker core, $\mathbf{A}_m \in \mathbb{R}^{D_m \times R_m}$ are the mode- m loading ma-

trices with $R_m \ll D_m$, and \mathcal{V}_i captures variation not explained by the low-rank component. This representation preserves the multiway structure of the original covariate, enabling the core channel to learn global multilinear dependencies directly from a low-dimensional latent tensor, and is well-suited when the tensor modes exhibit rich, simultaneous interactions.

CP-Core Adaptation. The CP variant decomposes \mathcal{X}_i as

$$\mathcal{X}_i = S(\mathcal{C}_i) + \mathcal{V}_i = \sum_{r=1}^R c_{i,r} \mathbf{a}_{1r} \circ \mathbf{a}_{2r} \circ \cdots \circ \mathbf{a}_{Mr} + \mathcal{V}_i, \quad (5)$$

where \circ denotes the outer product, $\{\mathbf{a}_{mr} \in \mathbb{R}^{D_m}\}_{r=1}^R$ are unit-norm mode- m factor vectors, and the latent core \mathcal{C}_i is represented by the coefficients $\{c_{i,r}\}_{r=1}^R$ via a super-diagonal tensor core whose nonzero entries correspond to these coefficients. The CP core is more parsimonious than Tucker’s core. Unlike Tucker, CP does not require orthogonal loading matrices, allowing the factor vectors to be collinear, which provides greater flexibility and interpretability as each component corresponds to a rank-1 outer product contribution.

Tensor-Train Core Adaptation. The Tensor-Train (TT) variant (Oseledets 2011) offers an alternative instantiation where \mathcal{X}_i is expressed as a sequence of third-order TT cores:

$$\mathcal{X}_i(i_1, \dots, i_M) = \mathcal{C}_i^{(1)}(1, i_1, :) \mathcal{C}_i^{(2)}(:, i_2, :) \cdots \mathcal{C}_i^{(M-1)}(:, i_{M-1}, :) \mathcal{C}_i^{(M)}(:, i_M, 1) + \mathcal{V}_i, \quad (6)$$

where $\mathcal{C}_i^{(m)} \in \mathbb{R}^{R_{m-1} \times D_m \times R_m}$ denotes the m -th TT core with boundary conditions $R_0 = R_M = 1$. The collection of TT cores $\mathcal{C}_i := \{\mathcal{C}_i^{(1)}, \dots, \mathcal{C}_i^{(M)}\}$ is processed through *embedded tensor-train layers (E-TTL)*, a multi-channel extension of the DC-TNN framework, where the refinement representation \mathcal{U}_i induced by \mathcal{V}_i is incorporated as an additional TT core. This augmented TT chain enables interactions both among TT cores and between the core and refinement component, while preserving the TT-rank structure. The sequential chain structure naturally captures hierarchical dependencies between modes. The detailed E-TTL architecture is presented in Appendix G.

Together, the Tucker, CP, and TT adaptations cover a broad spectrum of low-rank tensor structures, from multilinear factorizations to sequential tensor-train representations, providing a unified framework where the core channel captures structured global interactions and the refinement channel provides complementary sparse flexibility. The appropriate adaptation is selected via the data-driven procedure developed in Section 6.

3 Training of Dual-Channel Tensor Neural Networks

Two training procedures are developed for the DC-TNN framework, with the two-stage procedure presented in this section and an alternative end-to-end procedure in Appendix C (Tucker and CP) and Appendix G (TT). In the two-stage procedure, the core tensor $\tilde{\mathcal{C}}_i$ is first estimated outside the network by projecting \mathcal{X}_i onto estimated loading matrices via the inverse of $\mathcal{S}(\cdot)$, and then fixed during network training. This separation is adopted for theoretical convenience: under mild regularity conditions, standard estimators such as HOSVD (Zhang & Xia 2018) for Tucker and ALS (Anandkumar et al. 2015) for CP, achieve consistent core estimation, making it analytically tractable to characterize how estimation error propagates through the dual-channel network, as formalized in Theorem 5. In the end-to-end procedure, the decomposition parameters defining $\mathcal{S}(\cdot)$, is jointly optimized with the network weights and sparse refinement selector in a single training pipeline. Proposition 4 in Appendix C further establishes that with warm start and a local stability condition, the two-stage and end-to-end procedures are locally asymptotically equivalent.

In the two-stage procedure, the core tensor $\tilde{\mathcal{C}}_i$ is estimated from \mathcal{X}_i via the estimated inverse of the signal map $\hat{\mathcal{S}}^{-1}(\cdot)$, which admits a closed-form expression involving learned projection operators for Tucker and CP decompositions. With $\tilde{\mathcal{C}}_i$ fixed, the network parameters and refinement selector \mathcal{W}_u are jointly optimized. Rather than estimating the

refinement component as the residual $\mathcal{X}_i - \widehat{\mathcal{S}}(\widetilde{\mathcal{C}}_i)$, which is high-dimensional and sensitive to core estimation error, making error propagation through the network analytically challenging, we instead obtain the refinement representation directly via $\mathcal{U}_i = \mathcal{W}_u \bullet \mathcal{X}_i$. Here \mathcal{W}_u is a learned selection tensor with sparsity constraints that extracts a sparse and low-dimensional refinement input directly from \mathcal{X}_i . This design also makes the interaction between the core and refinement components explicit: while $\widetilde{\mathcal{C}}_i$ captures the global low-rank structure, \mathcal{W}_u implicitly models the complementary local structure by learning which coordinates of \mathcal{X}_i carry predictive information beyond what the core explains. We define the approximate effective dimension as $\mathbf{d}_{\text{in}} = (\bar{R}_1, \dots, \bar{R}_M, \bar{K}_1, \dots, \bar{K}_M)$, where $\bar{R}_m \geq R_m$ are possibly over-specified ranks and \bar{K}_m control the dimensionality of the refinement component. The joint optimization solves

$$\begin{aligned} \widehat{f}_n, \widehat{\mathcal{W}}_u \in & \arg \min_{\substack{f \in \mathcal{F}(L, \mathbf{d}_{\text{in}}, \mathbf{1}, \mathbf{d}_{\text{app}}, V, B) \\ \mathcal{W}_u \in \mathbb{R}^{\times_{m=1}^M \bar{K}_m \times_{m=1}^M D_m}}} (\mathcal{R}_n(f, \mathcal{W}_u) + \mathcal{P}_n(\mathcal{W}_u; \rho_\lambda)), \\ \mathcal{R}_n(f, \mathcal{W}_u) = & \frac{1}{n} \sum_{i=1}^n \left(y_i - f(\widetilde{\mathcal{C}}_i, \mathcal{W}_u \bullet \mathcal{X}_i) \right)^2, \quad \mathcal{P}_n(\mathcal{W}_u; \rho_\lambda) = \sum_{\mathcal{I}=(i_1, \dots, i_{2M})} \rho_\lambda((\mathcal{W}_u)_{\mathcal{I}}), \end{aligned} \quad (7)$$

where the hidden layer widths are all the same with $\mathbf{d}_{\text{app}} = (\widetilde{R}_1, \dots, \widetilde{R}_M, \widetilde{K}_1, \dots, \widetilde{K}_M)$, and $\rho_\lambda : \mathbb{R} \rightarrow [0, \infty)$ is a coordinate-wise penalty (e.g., ℓ_1 , clipped- L_1 , lasso, SCAD). Throughout the paper, the default choice is clipped- L_1 with the clipping threshold $\tau > 0$:

$$\rho_\lambda(\mathcal{X}) = \lambda \psi_\tau(\mathcal{X}), \quad \psi_\tau(\mathcal{X}) = \frac{|x|}{\tau} \wedge 1.$$

Core estimation error propagation. Since $\widetilde{\mathcal{C}}_i$ is a plug-in estimate of \mathcal{C}_i , the core estimation error propagates into the dual-channel learning procedure. We focus on the Tucker decomposition; the CP case follows analogously. For Tucker, the loading matrices $\{\mathbf{A}_m\}_{m=1}^M$ are first estimated as $\{\widehat{\mathbf{A}}_m \in \mathbb{R}^{\bar{R}_m \times D_m}\}_{m=1}^M$ via HOSVD, and the core is then estimated by projecting \mathcal{X}_i onto these estimated loadings: $\widetilde{\mathcal{C}}_i = \mathcal{X}_i \times_{m=1}^M \widehat{\mathbf{A}}_m^\top$. Substituting $\mathcal{X}_i = \mathcal{C}_i \times_{m=1}^M \mathbf{A}_m + \mathcal{V}_i$ gives

$$\tilde{\mathcal{C}}_i = (\mathcal{C}_i \times_{m=1}^M \mathbf{A}_m + \mathcal{V}_i) \times_{m=1}^M \hat{\mathbf{A}}_m^\top = \mathcal{C}_i \times_{m=1}^M (\hat{\mathbf{A}}_m^\top \mathbf{A}_m) + \mathcal{V}_i \times_{m=1}^M \hat{\mathbf{A}}_m^\top.$$

Setting $\mathbf{G}_m = \hat{\mathbf{A}}_m^\top \mathbf{A}_m \in \mathbb{R}^{\bar{R}_m \times R_m}$ and $\Xi = \mathcal{V}_i \times_{m=1}^M \hat{\mathbf{A}}_m^\top$, we obtain $\tilde{\mathcal{C}} = \mathcal{C} \times_1^M \mathbf{G}_m + \Xi$, where Ξ captures the projection of the local residual \mathcal{V}_i onto the estimated loading matrices. By the Lipschitzness of f and $\tilde{\mathcal{C}} \times_{m=1}^M \mathbf{G}_m^\dagger - \mathcal{C} = \Xi \times_{m=1}^M \mathbf{G}_m^\dagger$, where \mathbf{G}_m^\dagger is left inverse of \mathbf{G}_m ,

$$|f(\tilde{\mathcal{C}}, \mathcal{U}) - f(\mathcal{C}, \mathcal{U})| \lesssim \left\| \tilde{\mathcal{C}} \times_{m=1}^M \mathbf{G}_m^\dagger - \mathcal{C} \right\|_F = \left\| \Xi \times_{m=1}^M \mathbf{G}_m^\dagger \right\|_F \leq \prod_{m=1}^M \sigma_{\min}(\mathbf{G}_m)^{-1} \cdot \|\Xi\|_F.$$

A formal bound on $\mathbb{E}[\|\Xi\|_F^2]$ is established in Theorem 5.

Algorithm 1: Two-Stage Training of Dual-Channel Tensor Neural Networks

Input: Training set $\{(\mathcal{X}_i, y_i)\}_{i=1}^n$; decomposition type $\text{type} \in \{\text{Tucker}, \text{CP}\}$; network depth L ; layer widths $\{\mathbf{d}^{(\ell)}\}_{\ell=1}^L \cup \{d^{(L+1)}\}$; truncation level V ; Tucker/CP ranks $\{\bar{R}_m\}_{m=1}^M / \bar{R}$; refinement dimensions $\{\bar{K}_m\}_{m=1}^M$; penalty ρ_λ ; activation function α

Output: Learned predictor \hat{f}_n , selector $\widehat{\mathcal{W}}_u$, and residuals $\{\hat{r}_i\}_{i=1}^n$

- 1 Compute core representations $\tilde{\mathcal{C}}_i = \hat{\mathcal{S}}^{-1}(\mathcal{X}_i)$ for all $i \in [n]$ as follows
 - 2 **if** $\text{type} = \text{Tucker}$ **then**
 - 3 Compute orthonormal projection matrices $\{\hat{\mathbf{A}}_m\}_{m=1}^M$ via HOSVD
 - 4 Compute cores $\tilde{\mathcal{C}}_i = \mathcal{X}_i \times_{m=1}^M \hat{\mathbf{A}}_m^\top$ for all $i \in [n]$
 - 5 **else if** $\text{type} = \text{CP}$ **then**
 - 6 Run ALS to obtain normalized factor matrices $\{\hat{\mathbf{A}}_m \in \mathbb{R}^{d_m \times \bar{R}}\}_{m=1}^M$
 - 7 Compute the coefficient vector $\hat{\mathbf{c}}_i \in \mathbb{R}^{\bar{R}}$ by $\hat{\mathbf{c}}_i = \hat{\mathbf{G}}^{-1} \hat{\mathbf{m}}_i$, where $\hat{\mathbf{m}}_i(r) = \langle \mathcal{X}_i, \hat{\mathbf{a}}_{1r} \otimes \cdots \otimes \hat{\mathbf{a}}_{Mr} \rangle$, $\hat{\mathbf{G}} = \ast_{m=1}^M (\hat{\mathbf{A}}_m^\top \hat{\mathbf{A}}_m)$, with \ast denoting the Hadamard product
 - 8 Set $\tilde{\mathcal{C}}_i \leftarrow \hat{\mathbf{c}}_i$ for all $i \in [n]$
- 10 Obtain $(\hat{f}_n, \widehat{\mathcal{W}}_u)$ by solving

$$(\hat{f}_n, \widehat{\mathcal{W}}_u) \in \arg \min_{f \in \mathcal{F}(L, \{\mathbf{d}^{(\ell)}\}_{\ell=1}^L \cup \{d^{(L+1)}\}, V, B), \mathcal{W}_u \in \mathbb{R}^{\bar{K}_1 \times \cdots \times \bar{K}_M \times \prod_{m=1}^M D_m}} \{\mathcal{R}_n(f, \mathcal{W}_u) + \mathcal{P}_n(\mathcal{W}_u; \rho_\lambda)\},$$

- 11 where $\mathcal{R}_n(f, \mathcal{W}_u)$ and $\mathcal{P}_n(\mathcal{W}_u; \rho_\lambda)$ are defined in (7)
 - 12 Record residuals $\hat{r}_i \leftarrow \hat{y}_i - y_i$ for each $i \in [n]$
 - 13 **return** $\hat{f}_n, \widehat{\mathcal{W}}_u$, and $\{\hat{r}_i\}_{i=1}^n$
-

4 Statistical Guarantees for Prediction

This section establishes finite-sample risk bounds for the DC-TNN estimator. We show that under the core-refinement formulation, the estimator achieves optimal nonparametric rates, where the effective dimension depends on both the low-rank core and sparse refinement components. The resulting error decomposes into three interpretable terms: (i) approximation error of the neural network class, (ii) error propagated from estimating the latent low-rank structure, and (iii) complexity from sparse refinement selection. Together, these terms highlight how the dual-channel design reduces the intrinsic dimension of the problem compared to models relying on a single structural assumption.

4.1 Model Formulation and Assumptions

Let $\mathcal{X} \in \mathbb{R}^{\times_{m=1}^M D_m}$ denote a tensor covariate and $y \in \mathbb{R}$ (or $\{0, 1\}$ for binary classification) the response. The general regression function $f^*(\mathcal{X}) = \mathbb{E}[y \mid \mathcal{X}]$ minimizes the population L^2 risk $R(f) = \mathbb{E}[(y - f(\mathcal{X}))^2] = \int |y - f(\mathcal{X})|^2 \mu(d\mathcal{X}, dy)$, but directly learning f^* from \mathcal{X} is challenging due to the high ambient dimension $D_{\text{tot}} = \prod_{m=1}^M D_m$. We instead rewrite the model in the *core-refinement form*

$$y = f^*(\mathcal{C}, \mathcal{V}_{\mathcal{J}}) + \varepsilon, \quad \mathbb{E}[\varepsilon \mid \mathcal{C}, \mathcal{V}_{\mathcal{J}}] = 0,$$

where \mathcal{C} captures global low-rank structure and the response depends on \mathcal{V} only through the sparse index set $\mathcal{J} \subset [D_1] \times \cdots \times [D_M]$, so that $\mathcal{V}_{\mathcal{J}}$ encodes the localized variations relevant for prediction.

We impose the following assumptions, which are standard in tensor analysis and non-parametric regression, and ensure regularity of the learning problem. We focus on the Tucker instantiation; the analogous conditions for CP are provided in Appendix B.

Structural Assumptions (Tensor Decomposition). We assume the signal map $\mathcal{S}(\cdot)$

corresponds to a standard low-rank tensor factorization (Tucker or CP), with well-conditioned loading matrices and bounded latent core, ensuring the multilinear mapping is stable and invertible up to affine transformations. When the true ranks are known, the latent core can be *consistently recovered* (up to affine transformation) via HOSVD or HOOI. In practice, the true ranks are often unknown; Condition 2(iv) allows mild over-parameterization by working with $\bar{R}_m \geq R_m$, at the cost of an additional residual Ξ that vanishes as the ambient dimensions grow, as established in Theorem 5. The formal conditions are stated below.

Condition 2 (Tensor Factor Model). *For the Tucker factor model (4), we assume:*

(i)[**Well-conditioned loadings.**] *There exist constants $c_+ \geq c_- > 0$ such that the largest and the smallest singular values of each loading matrix \mathbf{A}_m satisfy $c_- D_m^{1/2} \leq \sigma_{\min}(\mathbf{A}_m) \leq \sigma_1(\mathbf{A}_m) \leq c_+ D_m^{1/2}$.*

(ii)[**Core recovery.**] *If the true ranks $\{R_m\}_{m=1}^M$ are used, the estimated orthonormal loading matrices $\tilde{\mathbf{A}}_m \in \mathbb{R}^{D_m \times R_m}$ obtained via HOSVD span the true loading subspaces with high probability, and the latent core \mathcal{C} can be consistently recovered up to affine transformation via $\tilde{\mathcal{C}} = \prod_{m=1}^M \mathcal{X} \times_{m=1}^M \tilde{\mathbf{A}}_m^\top$.*

(iii)[**Bounded core.**] *The latent core tensor satisfies $\|\mathcal{C}\|_F = \mathcal{O}(1)$.*

(iv)[**Over-parameterization.**] *For each mode m , choose $\bar{R}_m \geq R_m$ and let $\hat{\mathbf{A}}_m \in \mathbb{R}^{D_m \times \bar{R}_m}$ be a semi-orthogonal matrix obtained via HOSVD. Define $\mathbf{G}_m = \hat{\mathbf{A}}_m^\top \mathbf{A}_m \in \mathbb{R}^{\bar{R}_m \times R_m}$, then $\text{rank}(\mathbf{G}_m) = R_m$ and $c_- \leq \sigma_{\min}(\mathbf{G}_m) \leq \sigma_1(\mathbf{G}_m) \leq c_+$.*

Remark 2. Conditions 2 (i) and 2 (iii) are standard in tensor decomposition literature (Zhang & Xia 2018, Chen et al. 2024). We directly impose Condition 2 (ii) which ensures the signal term $\prod_{m=1}^M \mathcal{C} \times_{m=1}^M (\mathbf{A}_m \tilde{\mathbf{A}}_m^\top)$ dominates the noise term $\prod_{m=1}^M \mathcal{V} \times_{m=1}^M \tilde{\mathbf{A}}_m^\top$ so the latent core can be reliably recovered. Equivalently, one could assume a signal-to-noise ratio and apply the Davis-Kahan theorem, but we omit this for simplicity.

Smoothness of the Regression Function. We assume the true regression function f^* is bounded and smooth over the space $(\mathcal{C}, \mathcal{V}_{\mathcal{J}})$, where the *effective dimension* is $d_{\text{eff}} = \prod_{m=1}^M R_m + |\mathcal{J}|$. Condition 3 specifies boundedness and Lipschitz continuity of f^* , which controls its global behavior; Condition 4 specifies Hölder smoothness, which controls the local regularity of its higher-order derivatives and enables approximation by neural networks.

Condition 3 (Regression function). *The true regression function f^* satisfies $\|f^*\|_{\infty} \leq V^*$ and m^* is c -Lipschitz for some universal constants V^* and c . We further assume that $1 \leq V^* \leq V \leq c'V^*$ for some universal constant $c' > 1$.*

Condition 4 (Hölder smoothness of f^*). *The true regression function f^* belongs to a (β, C) -Hölder class with effective dimension d_{eff} . Specifically, let $\beta = a + b$ for some nonnegative integer a and $0 < b \leq 1$, and $C > 0$. For every multi-index $\alpha \in \mathbb{N}^d$ such that $\sum_{j=1}^{d_{\text{eff}}} \alpha_j = r$, the partial derivative $(\partial f^*)/(\partial \mathbf{x}_1^{\alpha_1} \cdots \partial \mathbf{x}_{d_{\text{eff}}}^{\alpha_{d_{\text{eff}}}})$ exists and satisfies*

$$\left| \frac{\partial^r f^*}{\partial \mathbf{x}_1^{\alpha_1} \cdots \partial \mathbf{x}_{d_{\text{eff}}}^{\alpha_{d_{\text{eff}}}}(\mathbf{z})} - \frac{\partial^r f^*}{\partial \mathbf{x}_1^{\alpha_1} \cdots \partial \mathbf{x}_{d_{\text{eff}}}^{\alpha_{d_{\text{eff}}}}(\mathbf{z}')} \right| \leq C \|\mathbf{z} - \mathbf{z}'\|_2^s,$$

where $\mathbf{x} = (\text{vec}(\mathcal{C})^\top, \text{vec}(\mathcal{V}_{\mathcal{J}})^\top)^\top$.

Regularity Conditions (Boundedness, Dependence, and Noise). We assume the entries of both the core tensor \mathcal{C} and refinement component $\mathcal{V}_{\mathcal{J}}$ are uniformly bounded, the refinement component satisfies a weak dependence condition across tensor entries, the noise ε is sub-Gaussian conditional on $(\mathcal{C}, \mathcal{V}_{\mathcal{J}})$, and \mathcal{C} and $\mathcal{V}_{\mathcal{J}}$ satisfy a weak dependence condition between each other. These assumptions are standard in high-dimensional nonparametric regression and ensure concentration of empirical processes and stability of estimation. The detailed conditions are provided in Appendix B.

Under these assumptions, we proceed to establish finite-sample guarantees for the DC-TNN estimator.

4.2 Finite-Sample Risk Bounds for DC-TNN

We now establish finite-sample guarantees for the DC-TNN estimator. Let $\widehat{f}(\mathcal{X})$ denote the DC-TNN estimator obtained from the two-stage training procedure in Section 3. Under the assumptions in Section 4.1, the following finite-sample risk bound holds.

Theorem 5 (Optimal rate for the DC-TNN estimator). *Work in the Tucker DC-TNN model under Conditions 2-4 and 1-3. Let $\mathcal{F}(L, \mathbf{d}_{in}, 1, \mathbf{d}_{app}, V, B)$ be the DC-TNN class with $\mathbf{d}_{app} = (\widetilde{R}_1, \dots, \widetilde{R}_M, \widetilde{K}_1, \dots, \widetilde{K}_M)$. We further denote $W = \prod_{m=1}^M \widetilde{R}_m + \prod_{m=1}^M \widetilde{K}_m$ and $Q = (\prod_m \bar{K}_m)(\prod_m D_m)$. Let \widehat{f} and $\widehat{\mathcal{W}}_u$ be any δ_{opt} -approximate empirical risk minimizers*

$$\widehat{f}\left(\mathcal{X}; [\widetilde{\mathbf{A}}_m]_{m=1}^M\right), \widehat{\mathcal{W}}_u \in \underset{\substack{f \in \mathcal{F}(L, \mathbf{d}_{in}, 1, \mathbf{d}_{app}, V, B) \\ \mathcal{W}_u \in \mathbb{R}^{\times_{m=1}^M K_m \times_{m=1}^M D_m}}}{\arg \min} \left\{ \mathcal{R}_n(f, \mathcal{W}_u) + \mathcal{P}_n(\mathcal{W}_u; \rho_\lambda) \right\} \quad \text{up to } \delta_{opt},$$

where $\mathcal{R}_n, \mathcal{P}_n$ are defined in (7), and $\rho_\lambda = \lambda \psi_\tau$ is chosen to be clipped- L_1 . Assume the depth $L = O(1)$ and the tuning parameters obey $\lambda \geq c_1 \frac{\log Qn + L \log(B(W+1))}{n}$ and $\tau^{-1} \geq c_2 (B(W+1))^{L+1} Qn$ for some universal constants $c_1, c_2 > 0$. Then, for $\forall t > 0$, with probability at least $1 - 3e^{-t}$,

$$\mathbb{E} \left| \widehat{f}(\mathcal{X}) - f^*(\mathcal{C}, \mathcal{V}_{\mathcal{J}}) \right|^2 \lesssim \underbrace{W^{-2\beta/d_{\text{eff}}}}_{\text{network approx.}} + \underbrace{\gamma^{-2} \frac{\sum_{m=1}^M \bar{R}_m D_m}{\prod_{m=1}^M D_m}}_{\text{core propagation}} + \underbrace{\Lambda_n + \lambda |\mathcal{J}|}_{\text{model/selector complexity}} + \delta_{opt} + \frac{t}{n},$$

where $\Lambda_n \asymp \frac{LW^2[L \log(B(W+1)) + \log n]}{n}$, β is from Condition 4 with the effective dimension $d_{\text{eff}} = \prod_{m=1}^M R_m + |\mathcal{J}|$.

Detailed proofs are provided in Section D of the supplemental material.

Error Decomposition and Interpretation. The bound decomposes the prediction error into three interpretable components:

- *Approximation error.* The term $W^{-2\beta/d_{\text{eff}}}$ reflects the expressive power of the neural network class in approximating the true regression function. It depends on the

effective dimension d_{eff} , which combines the low-rank and sparse components.

- *Core estimation error.* The term $\mathcal{E}_{\text{core}}$ quantifies the error introduced by estimating the latent core tensor C from the observed tensor X . This term captures how uncertainty in the low-rank structure propagates into prediction.
- *Model complexity and selection cost.* The term $\Lambda_n + \lambda|J|$ reflects the statistical complexity of the neural network and the cost of selecting relevant refinement features. The sparsity penalty controls the size of the active refinement set J , thereby regularizing the model.

Remark 3. Theorem 5 highlights a key advantage of the dual-channel framework: the effective dimension governing the learning rate is $d_{\text{eff}} = \prod_{m=1}^M R_m + |J|$, which can be substantially smaller than the ambient tensor dimension $\prod_{m=1}^M D_m$. As a result, the DC-TNN estimator avoids the curse of dimensionality by leveraging both low-rank structure and sparse refinement.

Moreover, the decomposition explicitly separates the effects of function approximation, structure estimation, and feature selection, providing a clear understanding of how each component contributes to the overall error. This structure is unique to the dual-channel formulation and is not available in models that rely solely on low-rank or sparse assumptions.

4.3 Optimal Rates and Effective Dimension

We now specialize the bound in Theorem 5 to derive optimal convergence rates and characterize the role of the hybrid structure through the effective dimension. By appropriately choosing the network width and regularization parameters, the DC-TNN estimator achieves the following rate.

Corollary 6. *Under the conditions of Theorem 5, suppose the network width is chosen as $W^* \asymp \left(\frac{n}{\log n}\right)^{d_{\text{eff}}/(2\beta+d_{\text{eff}})}$ and $\lambda^* \asymp \frac{\log Q + L \log(B(W^*+1))}{n} \asymp \frac{\log Q + \log n}{n}$, and further assume that the optimization error δ_{opt} is of smaller order, then we obtain the optimal risk rate:*

$$\mathbb{E} \left| \widehat{f}(\mathcal{X}) - f^*(\mathcal{C}, \mathcal{V}_{\mathcal{J}}) \right|^2 \lesssim \left(\frac{\log n}{n} \right)^{\frac{2\beta}{2\beta+d_{\text{eff}}}} + \gamma^{-2} \frac{\sum_{m=1}^M \bar{R}_m D_m}{\prod_{m=1}^M D_m} + \frac{|\mathcal{J}|(\log Q + \log n)}{n}.$$

Remark 4. Theorem 5 and Corollary 9 establish that the DC-TNN estimator achieves the minimax-optimal risk rate for nonparametric regression while explicitly accounting for both low-rank and sparse tensor structures. The bound decomposes into three interpretable components: (i) the *network approximation* term reflects the expressive power of the dual-channel network class; (ii) the *core propagation* term quantifies error from estimating the latent low-rank subspace; and (iii) the *model complexity* term captures the statistical cost of sparsity selection in the refinement channel. Together, these results show that leveraging the core-refinement architecture yields faster convergence and tighter generalization bounds than conventional tensor neural networks that rely solely on low-rank representations.

4.4 Why Dual-Channel Modeling Improves Prediction

The theoretical results above provide insight into why the proposed dual-channel architecture leads to improved predictive performance in heterogeneous tensor settings. In particular, the error decomposition in Theorem 5 reveals that the DC-TNN framework effectively balances two competing objectives: capturing global structure and preserving local flexibility.

Bias-Variance Tradeoff under Structural Modeling. A central challenge in tensor learning is the tradeoff between structural bias and statistical variance: Low-rank models impose strong global structure, reducing dimensionality and variance, but may suffer from

representation bias when localized signals are not aligned with the low-rank subspace. High-dimensional or sparse models offer flexibility to capture local effects, but operate in a large ambient space, leading to inflated effective dimension and higher variance.

The dual-channel formulation addresses this tradeoff by decomposing the input into a low-rank core and a sparse refinement component, and modeling them jointly. As reflected in the effective dimension $d_{\text{eff}} = \prod_{m=1}^M R_m + |J|$, the model achieves dimensionality reduction through the core while retaining flexibility through the refinement.

Error Decomposition Perspective. The finite-sample risk bound highlights three sources of error: approximation error, governed by the effective dimension d_{eff} ; core estimation error, arising from recovering the latent low-rank structure; and model complexity, driven by the size of the refinement set J . This decomposition shows that the dual-channel architecture allows these components to be controlled separately. In contrast, models based solely on low-rank or sparse assumptions entangle these effects, limiting their ability to adapt to heterogeneous data.

Adaptivity to Heterogeneous Structure. The DC-TNN framework adapts naturally to different structural regimes: When the data are primarily low-rank, the refinement component becomes negligible, and the model reduces to a low-dimensional representation with strong statistical efficiency; When localized effects are important, the refinement channel selectively incorporates relevant features, avoiding the need to model the entire tensor space. This adaptivity enables the model to achieve near-optimal performance across a broad class of data-generating mechanisms, without requiring prior knowledge of the true structure.

Comparison with Single-Structure Models. The above analysis explains why the dual-channel approach outperforms models that rely on a single structural assumption:

Compared to pure low-rank tensor models, DC-TNN avoids bias introduced by unmodeled local effects; Compared to high-dimensional or sparse models, DC-TNN reduces variance by exploiting low-rank structure; Compared to existing tensor neural networks, which typically adopt a single decomposition, DC-TNN provides a strictly richer function class that can represent both global and local patterns.

In summary, the dual-channel architecture improves prediction by combining the strengths of low-rank and sparse modeling while mitigating their respective weaknesses. The theoretical guarantees show that this hybrid structure leads to reduced effective dimension, improved approximation capability, and optimal statistical rates, providing a principled foundation for modeling heterogeneous tensor data.

5 Structure-Aware Uncertainty Quantification

In many applications, predictive performance is evaluated using ROC curves, sensitivity, specificity, and the area under the curve (AUC) (Fawcett 2006, Majnik & Bosnić 2013). While point estimates of these quantities are widely used, they do not capture uncertainty arising from finite samples and model estimation, which is critical for reliable decision-making.

Standard approaches to uncertainty quantification for ROC curves include bootstrap methods and parametric modeling assumptions (Nakas et al. 2023). However, bootstrap-based procedures have been shown to be unreliable in classification settings, and parametric approaches are often misspecified in high-dimensional tensor problems (Zheng et al. 2025). Recent advances based on conformal prediction provide a distribution-free alternative, but existing methods typically treat tensor inputs as unstructured vectors, ignoring their underlying structure (?Zheng et al. 2024).

As a result, applying standard conformal methods directly to tensor data often leads to overly conservative and less informative uncertainty estimates, since the calibration step does not exploit the intrinsic geometry of the data.

5.1 Structure-Aware Conformal Inference

To address this limitation, we develop a structure-aware conformal inference framework that leverages the core-refinement decomposition of the DC-TNN model. We present the method in a binary classification problem with outcome $y \in \{0, 1\}$. The framework can be readily extended to a K -class classification setting by constructing $(K - 1)$ ROC curves, each comparing one category against all others (Everson & Fieldsend 2006).

We randomly split the dataset $\mathcal{D} = \{(\mathcal{X}_i, y_i)\}_{i=1}^n$ into training, calibration, and test sets $\mathcal{D}_{\text{tr}}, \mathcal{D}_{\text{ca}}, \mathcal{D}_{\text{tst}}$, with corresponding index sets $\mathcal{I}_{\text{tr}}, \mathcal{I}_{\text{ca}}, \mathcal{I}_{\text{tst}}$ and sizes $n_{\text{tr}} = |\mathcal{I}_{\text{tr}}|, n_{\text{ca}} = |\mathcal{I}_{\text{ca}}|$, and $n_{\text{tst}} = |\mathcal{I}_{\text{tst}}|$. A DC-TNN model is trained on \mathcal{D}_{tr} , yielding predicted probabilities $\hat{\pi}(\mathcal{X}) = \hat{m}(\mathcal{C}, \mathcal{U})$, and construct conformal prediction intervals using a split conformal framework. We aim to construct *conditional prediction ROC (CP-ROC) bands* that quantify uncertainty in sensitivity (True Positive Rate) and specificity (True Negative Rate) across decision thresholds λ , defined as follows

$$\text{Sens}(\lambda) = \frac{1}{|\mathcal{I}_{\text{tst}}^{(1)}|} \sum_{j \in \mathcal{I}_{\text{tst}}^{(1)}} \mathbf{1}(\hat{\pi}(\mathcal{X}_j) > \lambda), \quad \text{Spec}(\lambda) = \frac{1}{|\mathcal{I}_{\text{tst}}^{(0)}|} \sum_{j \in \mathcal{I}_{\text{tst}}^{(0)}} \mathbf{1}(\hat{\pi}(\mathcal{X}_j) \leq \lambda).$$

For simplicity, we write $\hat{\pi}_i = \hat{\pi}(\mathcal{X}_i)$ when no ambiguity arises.

Step 1: Local calibration in core-refinement space. For each test point $j \in \mathcal{I}_{\text{tst}}$, construct a local calibration set $\mathcal{I}_{\text{ca},j}^{\text{loc}} \subset \mathcal{I}_{\text{ca}}$ using K -nearest neighbors under a distance

$$d_{CR}(i, j) = \|\hat{\mathcal{C}}(\mathcal{X}_i) - \hat{\mathcal{C}}(\mathcal{X}_j)\|_F + \omega \|\hat{\mathcal{U}}(\mathcal{X}_i) - \hat{\mathcal{U}}(\mathcal{X}_j)\|_F, \quad (8)$$

with given $\omega > 0$. This metric adapts to the two-channel decomposition: low-rank similarity

dominates when the signal is factor-driven, while selected idiosyncratic modes refine local neighborhoods.

Step 2: Class-conditional calibration. The ideal conformity score is defined as $s_i = \pi(\mathcal{X}_i) - \hat{\pi}_i$, where $\pi(\mathcal{X}_i) = \mathbb{P}(y = 1 \mid \mathcal{X}_i)$ denotes the true conditional probability. Since $\pi(\mathcal{X}_i)$ is not observable, we approximate it using a nonparametric estimator constructed in the core-refinement latent space.

Specifically, we define $\tilde{\pi}(\cdot)$ as a K_{tr} -nearest neighbor (KNN) smoother based on $\hat{\pi}$ over the training set \mathcal{D}_{tr} , where neighbors are selected according to the distance in (8). This yields a proxy $\tilde{\pi}(\mathcal{X}_i) = \tilde{\pi}(\hat{\mathcal{C}}(\mathcal{X}_i), \hat{\mathcal{U}}(\mathcal{X}_i))$ for $\pi(\mathcal{X}_i)$. The choice of K_{tr} is discussed in Remark 7.

For each $i \in \mathcal{I}_{ca,j}^{\text{loc}}$, we define the estimated conformity score $\tilde{s}_i = \tilde{\pi}(\hat{\mathcal{C}}(\mathcal{X}_i), \hat{\mathcal{U}}(\mathcal{X}_i)) - \hat{\pi}_i$, and construct the class-conditional calibration sets

$$\mathcal{S}_j^{(1)} = \{\tilde{s}_i : i \in \mathcal{I}_{ca,j}^{\text{loc}}, y_i = 1\}, \quad \mathcal{S}_j^{(0)} = \{\tilde{s}_i : i \in \mathcal{I}_{ca,j}^{\text{loc}}, y_i = 0\}.$$

Step 3: Conformal intervals for predicted probabilities. Let $q_\gamma^{(k)}(j)$ be the γ -quantile of $\mathcal{S}_j^{(k)}$. The class-conditional conformal interval for $\pi(\mathcal{X}_j)$ is

$$C_\alpha^{(k)}(\mathcal{X}_j) = [\hat{\pi}(\mathcal{X}_j) + q_{\alpha/2}^{(k)}(j), \hat{\pi}(\mathcal{X}_j) + q_{1-\alpha/2}^{(k)}(j)] \cap [0, 1], \quad k \in \{0, 1\}.$$

Step 4: Pointwise ROC confidence bands. We then combine all the individual intervals into the ROC confidence band and form the AUC confidence interval. Let $\mathcal{I}_{tst}^{(1)} = \{j \in \mathcal{I}_{tst} : y_j = 1\}$ and $\mathcal{I}_{tst}^{(0)} = \{j \in \mathcal{I}_{tst} : y_j = 0\}$, denote \underline{C} , \overline{C} as the lower and upper limit of an interval C . For threshold $\lambda \in [0, 1]$, obtain the confidence intervals for sensitivity and specificity by

$$C_\alpha^{\text{sens}}(\lambda) = \left[\frac{1}{|\mathcal{I}_{tst}^{(1)}|} \sum_{j \in \mathcal{I}_{tst}^{(1)}} \mathbf{1}\{\underline{C}_\alpha^{(1)}(\mathcal{X}_j) > \lambda\}, \frac{1}{|\mathcal{I}_{tst}^{(1)}|} \sum_{j \in \mathcal{I}_{tst}^{(1)}} \mathbf{1}\{\overline{C}_\alpha^{(1)}(\mathcal{X}_j) > \lambda\} \right],$$

$$C_\alpha^{\text{spec}}(\lambda) = \left[\frac{1}{|\mathcal{I}_{tst}^{(0)}|} \sum_{j \in \mathcal{I}_{tst}^{(0)}} \mathbf{1}\{\overline{C_\alpha^{(0)}}(\mathcal{X}_j) \leq \lambda\}, \frac{1}{|\mathcal{I}_{tst}^{(0)}|} \sum_{j \in \mathcal{I}_{tst}^{(0)}} \mathbf{1}\{C_\alpha^{(0)}(\mathcal{X}_j) \leq \lambda\} \right].$$

Varying λ over a grid for $C_\alpha^{\text{sens}}(\lambda)$ yields ROC confidence band for sensitivity and for $C_\alpha^{\text{spec}}(\lambda)$ yields ROC confidence band for specificity.

Step 5: AUC confidence intervals. For AUC, the two types of confidence intervals are calculated from the numerical integration of the upper and lower bounds of the ROC confidence bands, for either the sensitivity or the specificity.

$$C_{\text{auc}}^{\text{sens}}(\alpha) = \left[\int_0^1 \underline{C_\alpha^{\text{sens}}}(\text{Spec}^{-1}(1-x)) dx, \int_0^1 \overline{C_\alpha^{\text{sens}}}(\text{Spec}^{-1}(1-x)) dx \right]$$

$$C_{\text{auc}}^{\text{spec}}(\alpha) = \left[1 - \int_0^1 \overline{C_\alpha^{\text{spec}}}(\text{Sens}^{-1}(\mathcal{X})) dx, 1 - \int_0^1 \underline{C_\alpha^{\text{spec}}}(\text{Sens}^{-1}(\mathcal{X})) dx \right]$$

5.2 Theoretical Coverage Guarantees

We now establish the validity of the proposed structure-aware conformal procedure. We first define the oracle sensitivity and specificity as our target:

$$\text{Sens}_0(\lambda) = \frac{1}{|\mathcal{I}_{tst}^{(1)}|} \sum_{j \in \mathcal{I}_{tst}^{(1)}} \mathbf{1}(\pi(\mathcal{X}_j) > \lambda), \quad \text{Spec}_0(\lambda) = \frac{1}{|\mathcal{I}_{tst}^{(0)}|} \sum_{j \in \mathcal{I}_{tst}^{(0)}} \mathbf{1}(\pi(\mathcal{X}_j) \leq \lambda),$$

where $\pi(\mathcal{X}) = P(y = 1 \mid \mathcal{X})$ is the oracle success probability.

Proposition 7 (Coverage of structure-aware ROC bands). *Suppose for each $j \in \mathcal{I}_{tst}$ the local calibration set $\mathcal{I}_{ca,j}^{\text{loc}}$ is exchangeable with (\mathcal{X}_j, y_j) and $\lim_{n_{tr} \rightarrow \infty} \max_{j \in \mathcal{I}_{tst}} |\tilde{\pi}(\widehat{\mathcal{C}}(\mathcal{X}_j), \widehat{\mathcal{U}}(\mathcal{X}_j)) - \pi(\mathcal{X}_j)| = 0$. Then for randomly chosen $\lambda \in [0, 1]$,*

$$\lim_{n_{tr}, n_{ca}, n_{tst} \rightarrow \infty} \min \{P(\text{Sens}_0(\lambda) \in C_\alpha^{\text{sens}}(\lambda)), P(\text{Spec}_0(\lambda) \in C_\alpha^{\text{spec}}(\lambda))\} \geq 1 - 2\alpha$$

Additionally, if we further assume that the CDF of s_i with $y_i = k$, denoted as $F_k(\cdot)$, satisfies that $F_k^{-1}(\alpha/2) < 0$ and $F_k^{-1}(1 - \alpha/2) > 0$, then as $n_{tr}, n_{ca}, n_{tst} \rightarrow \infty$ almost surely, $\text{Sens}(\lambda) \in C_\alpha^{\text{sens}}(\lambda)$ and $\text{Spec}(\lambda) \in C_\alpha^{\text{spec}}(\lambda)$.

Remark 5 (Exchangeability under local calibration). The assumption that the local calibration set $\mathcal{I}_{\text{ca},j}^{\text{loc}}$ is exchangeable with the target point (\mathcal{X}_j, y_j) assumes that the nearest neighbors form a locally homogeneous sample. This condition is supported by the nearest-neighbor conformal prediction framework of Györfi & Walk (2019), where conditional coverage is achieved under a smooth conditional distribution of y_j given \mathcal{X}_j and an appropriately chosen k-NN algorithm.

Remark 6 (Consistency of probability estimation). The assumption in Proposition 7 requires that the estimated probability $\tilde{\pi}(\widehat{\mathcal{C}}(\mathcal{X}), \widehat{\mathcal{U}}(\mathcal{X}))$ approximates the true probability $\pi(\mathcal{X})$ uniformly over the test sample. This is stronger than classical L_1 -consistency of K -nearest neighbor regression, but is substantially weaker than requiring uniform convergence over the entire input space.

This requirement is motivated by performing probability smoothing in the core-refinement representation space rather than in the ambient tensor space. Once \mathcal{X} is mapped to $(\widehat{\mathcal{C}}(\mathcal{X}), \widehat{\mathcal{U}}(\mathcal{X}))$, the effective dimension is significantly reduced, making nonparametric approximation more stable. Under mild smoothness conditions on $\pi(\mathcal{X})$ as a function of this representation, consistency over the test sample becomes plausible. Remark 7 further clarifies this connection through standard nonparametric convergence rates.

Remark 7 (Choice of KNN parameters and connection to nonparametric rates).

Under additional smoothness assumptions, the consistency requirement in Proposition 7 can be related to standard nonparametric regression theory in the core-refinement representation space. Suppose $\pi(\mathcal{X})$ is (β, C) -Hölder continuous with respect to the metric induced by $(\widehat{\mathcal{C}}(\mathcal{X}), \widehat{\mathcal{U}}(\mathcal{X}))$, and that the representation has effective dimension $d_{\text{rep}} = \prod_{m=1}^M \bar{R}_m + \prod_{m=1}^M \bar{K}_m$. Then the K_{tr} -nearest neighbor estimator satisfies

$$\sup_{j \in I_{\text{tst}}} \left| \tilde{\pi}(\widehat{\mathcal{C}}(\mathcal{X}_j), \widehat{\mathcal{U}}(\mathcal{X}_j)) - \pi(\mathcal{X}_j) \right| = O_p \left(\left(\frac{K_{\text{tr}}}{n_{\text{tr}}} \right)^{\beta/d_{\text{rep}}} + K_{\text{tr}}^{-1/2} \right),$$

up to logarithmic factors and standard regularity conditions.

Balancing the bias and variance terms yields

$$K_{\text{tr}} \asymp n_{\text{tr}}^{\frac{2\beta}{2\beta+d_{\text{rep}}}}, \quad \max_{j \in I_{\text{tst}}} \left| \tilde{\pi}(\widehat{\mathcal{C}}(\mathcal{X}_j), \widehat{\mathcal{U}}(\mathcal{X}_j)) - \pi(\mathcal{X}_j) \right| = O_p \left(n_{\text{tr}}^{-\beta/(2\beta+d_{\text{rep}})} \right).$$

Thus, the assumption in Proposition 7 is most plausible when the learned representation is sufficiently low-dimensional and preserves the smoothness structure of $\pi(\mathcal{X})$. In the special case $\beta = 1$, this reduces to $K_{\text{tr}} \asymp n_{\text{tr}}^{2/(2+d_{\text{rep}})}$.

For local calibration, Györfi & Walk (2019) suggests that $K_{\text{tr}}/(\log(n_{\text{tr}}))^2 \rightarrow \infty$ and $K_{\text{tr}}(\log(n_{\text{tr}}))^{d_{\text{rep}}}/n \rightarrow 0$ to ensure consistent estimation of class-conditional quantiles. In practice, K_{tr} and K_{ca} are chosen to balance approximation accuracy and sufficient local sample size.

For the coverage rate of the AUC confidence intervals, similarly define the oracle AUC, denoted as AUC_0 , as the area under the oracle ROC curve defined by $\text{Sens}_0(\cdot)$ and $\text{Spec}_0(\cdot)$. And the theoretical coverage guarantee is given below.

Corollary 8 (AUC coverage from CP-ROC bands). *Assume the same conditions as in Proposition 7 hold, then*

$$\lim_{n_{\text{tr}}, n_{\text{ca}}, n_{\text{tst}} \rightarrow \infty} \min \left\{ P(\text{AUC}_0 \in C_{\text{auc}}^{\text{sens}}(\alpha)), P(\text{AUC}_0 \in C_{\text{auc}}^{\text{spec}}(\alpha)) \right\} \geq 1 - 2\alpha$$

The proofs are detailed in Section E in the supplemental material. The proposed uncertainty quantification framework leverages the same core-refinement structure used for prediction to construct *valid and informative confidence regions*. By calibrating in a structured feature space, the method improves upon standard conformal approaches and provides a principled way to quantify uncertainty in tensor-based predictive models.

6 Provable Low-Rank Structure Selection

Identifying the true low-rank structure of tensor features is a fundamental yet unresolved challenge: naive selection based on predictive accuracy or AUC lacks statistical validity and often leads to overfitting. We propose a *conformal ROC method* that leverages the DC-TNN’s core-refinement representation to construct finite-sample confidence bands for performance differences between candidate models. This procedure provides the first provably valid statistical test for selecting among Tucker, CP, or other low-rank tensor structures.

To illustrate the idea, we compare two fitted models, $\hat{f}^{(\text{Tucker})}$ and $\hat{f}^{(\text{CP})}$, trained on the same dataset. Specifically, we consider the following hypothesis test problem:

$$H_0 : \hat{f}^{(\text{CP})} \text{ outperforms } \hat{f}^{(\text{Tucker})}, H_a : \hat{f}^{(\text{CP})} \text{ no better than } \hat{f}^{(\text{Tucker})}.$$

Notice that the above hypothesis test protects the Null, meaning that we prefer $\hat{f}^{(\text{Tucker})}$ if there is no evidence that $\hat{f}^{(\text{CP})}$ is significantly better. On the other hand, if $\hat{f}^{(\text{CP})}$ is preferred, the symmetric hypothesis test can be adopted where $H_0 : \hat{f}^{(\text{Tucker})}$ outperforms $\hat{f}^{(\text{CP})}$. We focus on binary classification with $y \in \{0, 1\}$, noting that the approach generalizes to multi-class problems by constructing K ROC curves, one for each label $k = 1, \dots, K$.

6.1 Conformal ROC-Based Structure Selection for Classification

The dataset is partitioned into training, calibration, and test subsets, $\mathcal{D}_{tr} \cup \mathcal{D}_{ca} \cup \mathcal{D}_{tst}$. Models are trained on \mathcal{D}_{tr} to obtain $\hat{f}^{(\text{Tucker})}(\cdot | \mathcal{D}_{tr})$ and $\hat{f}^{(\text{CP})}(\cdot | \mathcal{D}_{tr})$, and the calibration set \mathcal{D}_{ca} is used to construct conformal confidence bands that support inference on the held-out test set \mathcal{D}_{tst} . For a fixed threshold $\lambda' \in [0, 1]$, the two models yield classifiers $\hat{y}^{(\text{Tucker})} = \mathbb{1}\{\hat{f}^{(\text{Tucker})}(\mathcal{X}) \geq \lambda'\}$ and $\hat{y}^{(\text{CP})} = \mathbb{1}\{\hat{f}^{(\text{CP})}(\mathcal{X}) \geq \lambda'\}$. A naive comparison would be based on the misclassification rate $\frac{1}{n_{tst}} \sum_{j \in \mathcal{I}_{tst}} 1(y_j \neq \hat{y})$, but this rate neglects

the potential effects arising from the choice of threshold λ' . By varying λ' , one obtains the ROC curves of both models, but direct statistical tests for comparing these curves under a fitted classifier setting are lacking. Existing methods for comparing ROC curves (DeLong et al. 1988, Venkatraman & Begg 1996) are tailored to diagnostic testing on fixed scores and do not account for the uncertainty introduced by model training.

To address this, we consider the difference in predictive scores

$$d(\mathcal{X}) = \hat{f}^{(Tucker)}(\hat{\mathcal{C}}^{(Tucker)}, \hat{\mathcal{U}}^{(Tucker)}) - \hat{f}^{(CP)}(\hat{\mathcal{C}}^{(CP)}, \hat{\mathcal{U}}^{(CP)}).$$

For each test point, $d(\mathcal{X})$ induces the contingency table Table 1, from which a ROC curve is constructed. To interpret this contingency table, if Tucker decomposition truly outperforms CP, then at any threshold λ we expect more positives to satisfy $d(\mathcal{X}) > \lambda$ and more negatives to satisfy $d(\mathcal{X}) \leq \lambda$. In terms of the contingency table, this corresponds to large $n_{11}(\lambda)$ and $n_{22}(\lambda)$, with comparatively small $n_{12}(\lambda)$ and $n_{21}(\lambda)$. As λ varies, the resulting ROC curve based on $d(\mathcal{X})$ will lie above the reference line $y = x$, indicating that Tucker systematically assigns higher scores to the true positives relative to CP. Conversely, if CP is superior, then $d(\mathcal{X})$ tends to be smaller for positives and larger for negatives, leading to an ROC curve that falls below the diagonal. When the two decompositions have comparable predictive ability, the difference curve will fluctuate around the diagonal, with no systematic dominance in sensitivity–specificity trade-offs.

	$d(\mathcal{X}) > \lambda$	$d(\mathcal{X}) \leq \lambda$
$y = 1$	$n_{11}(\lambda)$	$n_{12}(\lambda)$
$y = 0$	$n_{21}(\lambda)$	$n_{22}(\lambda)$

Table 1: Contingency table under our model comparison setup

To rigorously account for finite-sample variability, we can construct conformal confidence bands for the difference ROC curve with similar procedure as described in Section 5. These bands provide a formal guarantee: with probability at least $1 - \alpha$, the oracle

difference ROC curve is contained entirely within the band. If the band lies strictly above (or below) the diagonal, one can conclude that Tucker (or CP) is significantly better; if the band overlaps the diagonal, the two models are statistically indistinguishable. The procedure is summarized in Algorithm 2. A key component is the use of local calibration: for each test point \mathcal{X}_j , we form a neighborhood $\mathcal{N}_j = \{(\mathcal{X}_i, y_i) \in \mathcal{D}_{ca} : d_{FA}(\mathcal{X}_i, \mathcal{X}_j) \leq \delta, y_i = y_j\}$ based on a distance metric $d_{FA}(\cdot, \cdot)$ (8) in the core-refinement-augmented latent space. This ensures approximate exchangeability between calibration and test points, which is necessary for conformal validity of the ROC band.

6.2 Finite-Sample Guarantees for Structure Selection

We now establish the statistical validity of the proposed structure selector. First, we show that the conformal confidence intervals for the AUC achieve finite-sample coverage at the target confidence level. Second, we prove that, under mild regularity conditions, the selector is asymptotically consistent: if one of the low rank structure identifies the true structure of the data, then the selector will be able to select it.

Let $f^{(T)*}$ and $f^{(C)*}$ denote the population risk minimizers within the Tucker and CP classes, respectively, and write the *oracle difference score* as

$$\delta(\mathcal{X}) = f^{(T)*}(\mathcal{X}) - f^{(C)*}(\mathcal{X}).$$

For $\lambda \in \mathbb{R}$, define the *oracle difference sensitivity and specificity*:

$$\text{dSens}_0(\lambda) = \frac{1}{|\mathcal{I}_{tst}^{(1)}|} \sum_{j \in \mathcal{I}_{tst}^{(1)}} \mathbf{1}\{\delta(\mathcal{X}_j) > \lambda\}, \quad \text{dSpec}_0(\lambda) = \frac{1}{|\mathcal{I}_{tst}^{(0)}|} \sum_{j \in \mathcal{I}_{tst}^{(0)}} \mathbf{1}\{\delta(\mathcal{X}_j) \leq \lambda\}.$$

and the oracle AUC can be calculated by

$$\text{dAUC}_0 = \int_0^1 \text{dSens}_0((\text{dSpec}_0)^{-1}(1-x)) dx$$

Then we develop the theoretical coverage for the AUC confidence intervals as follows:

Algorithm 2: Model Selector

Input: Training set $\{(\mathcal{X}_i, y_i) : i \in \mathcal{I}_{tr}\}$, calibration set $\{(\mathcal{X}_i, y_i) : i \in \mathcal{I}_{ca}\}$ and test set $\{(\mathcal{X}_j, y_j) : i \in \mathcal{I}_{tst}\}$, split its index set by the label y : $\mathcal{I}_{tst,0}$ and $\mathcal{I}_{tst,1}$, significance level $\alpha \in (0, 1)$, output difference between the two models $d(\mathcal{X})$, k -NN selector $\mathcal{N}(\mathcal{X})$, grid value $-1 < \lambda_1 < \lambda_2 < \dots < \lambda_G \leq 1$

Output: Testing ROC curve band and its AUC confidence band.

1 **for** $j \in \mathcal{I}_{tst}$ **do**

2 Calculate the local calibration set $\mathcal{N}(\mathcal{X}_j) \subset \mathcal{D}_{ca}$ and denote

$$\mathcal{I}_{jk} = \{i : (\mathcal{X}_i, y_i) \in \mathcal{N}(\mathcal{X}_j), y_i = k\}$$

3 Calculate difference $d_i = d(\mathcal{X}_i)$, for $i \in \mathcal{I}_{jk}$ and $d_j = d(\mathcal{X}_j)$

4 Obtain conformal prediction interval for the differenced (\mathcal{X}_j) with $y_j = k$ as

$$dC_\alpha^{(k)}(\mathcal{X}_j) = [q_{\alpha/2}(\{d_i\}_{i \in \mathcal{I}_{jk}}), q_{1-\alpha/2}(\{d_i\}_{i \in \mathcal{I}_{jk}})].$$

5 **for** $g = 1, 2, \dots, G$ **do**

6 Calculate sensitivity and specificity for the difference as

$$dSens(\lambda_g) = \frac{1}{|\mathcal{I}_{tst,1}|} \sum_{j \in \mathcal{I}_{tst,1}} \mathbf{1}(d_j > \lambda_g), \quad dSpec(\lambda_g) = \frac{1}{|\mathcal{I}_{tst,0}|} \sum_{j \in \mathcal{I}_{tst,0}} \mathbf{1}(d_j \leq \lambda_g).$$

8 Calculate confidence intervals for sensitivity $Sens(\lambda_g)$ and specificity $Spec(\lambda_g)$

9 as

$$dC_\alpha^{sens}(\lambda_g) = \left[\frac{1}{|\mathcal{I}_{tst,1}|} \sum_{j \in \mathcal{I}_{tst,1}} \mathbf{1}(dC_\alpha^{(1)}(\mathcal{X}_j) > \lambda_g), \frac{1}{|\mathcal{I}_{tst,1}|} \sum_{j \in \mathcal{I}_{tst,1}} \mathbf{1}(\overline{dC_\alpha^{(1)}}(\mathcal{X}_j) > \lambda_g) \right],$$

$$dC_\alpha^{spec}(\lambda_g) = \left[\frac{1}{|\mathcal{I}_{tst,0}|} \sum_{j \in \mathcal{I}_{tst,0}} \mathbf{1}(\overline{dC_\alpha^{(0)}}(\mathcal{X}_j) \leq \lambda_g), \frac{1}{|\mathcal{I}_{tst,0}|} \sum_{j \in \mathcal{I}_{tst,0}} \mathbf{1}(dC_\alpha^{(0)}(\mathcal{X}_j) \leq \lambda_g) \right].$$

10

11

13 Calculate AUC confidence set as

$$dC_{auc}^{sens}(\alpha) = \left[\sum_{g=2}^G \overline{dC_\alpha^{sens}}(\lambda_{g-1}) [dSpec(\lambda_g) - dSpec(\lambda_{g-1})], \sum_{g=2}^G dC_\alpha^{sens}(\lambda_{g-1}) [dSpec(\lambda_g) - dSpec(\lambda_{g-1})] \right]$$

$$14 \quad dC_{auc}^{spec}(\alpha) = \left[\sum_{g=2}^G \overline{dC_\alpha^{spec}}(\lambda_g) [dSens(\lambda_{g-1}) - dSens(\lambda_g)], \sum_{g=2}^G dC_\alpha^{spec}(\lambda_g) [dSens(\lambda_{g-1}) - dSens(\lambda_g)] \right]$$

15

Theorem 9 (Validity of different AUC Conformal confidence intervals). *Assume for each $j \in \mathcal{I}_{tst}^{(k)}$: (i) local exchangeability—conditionally on \mathcal{X}_j and $y_j = k$, the multiset $\{(\mathcal{X}_i, y_i) : i \in \mathcal{I}_{ca,j}^{loc}, y_i = k\}$ is exchangeable with (\mathcal{X}_j, y_j) ; (ii) the conditional CDF of $s = \delta(\mathcal{X}) - d(\mathcal{X})$ given $(\mathcal{X}, y = k)$ is continuous. Then we have that*

$$\lim_{n_{ca}, n_{tst} \rightarrow \infty} \min \{P(dAUC_0 \in dC_{auc}^{sens}), P(dAUC_0 \in dC_{auc}^{spec})\} \geq 1 - 2\alpha$$

The proof follows a similar argument to that of Corollary 8, with full details provided in Section F of the supplemental material. Note that compare with Corollary 8, we do not need a k-NN estimator of $\tilde{\pi}(\cdot)$ as we directly target on the difference $d(\mathcal{X})$. Consequently, the assumptions here are weaker.

Now we are ready to choose the decision rule that define the structure selector. Notice that if Tucker structure has better predictive performance, the difference ROC curve should lie above the reference line $y = x$, thus we have that $dAUC_0 > 0.5$. We can then use the confidence interval dC_{auc}^{sens} to test the predictive performance of the two structures for samples with label $y = 1$, and use dC_{auc}^{spec} to test the predictive performance for samples with label $y = 0$. The detailed selector is given below:

- Sensitivity selector: Focus on sensitivity for positively labeled group, select Tucker if the lower bound of C_{auc}^{sens} is above 0.5; select CP if the upper bound of C_{auc}^{sens} is below 0.5; otherwise, declare a tie.
- Specificity selector: Focus on specificity for negatively labeled group, select Tucker if the lower bound of C_{auc}^{spec} is above 0.5; select CP if the upper bound of C_{auc}^{spec} is below 0.5; otherwise, declare a tie.

To develop theoretical consistency of the selector, assume the true low rank structure is either Tucker or CP, then intuitively, the other low rank structure won't be able to provide

better prediction than this true structure, thus our proposed selector is able to select the true structure with probability at the chosen confidence level $1 - \alpha$. The detailed theorem is given below, and its proof is provided in Section F in the supplemental material.

Theorem 10. (*False discovery rate control*) For $i \in \mathcal{I}_{\text{tst}}$, let $p^*(\mathcal{C}_i, \mathcal{U}_i) = \mathbb{E}[y_i = 1 \mid \mathcal{C}_i, \mathcal{U}_i]$.

Assume the Tucker-based predictor $\hat{f}^{(\text{Tucker})}(\hat{\mathcal{C}}_i^{(\text{Tucker})}, \hat{\mathcal{U}}_i^{(\text{Tucker})})$ is consistent in the sense that

$$\lim_{n_{tr} \rightarrow \infty} \mathbb{1} |\hat{f}^{(\text{Tucker})}(\hat{\mathcal{C}}_i^{(\text{Tucker})}, \hat{\mathcal{U}}_i^{(\text{Tucker})}) - p^*(\mathcal{C}_i, \mathcal{U}_i)| = 0. \quad (9)$$

If (9) holds for all $y_i = 1$, then

$$\lim_{n_{tr}, n_{ca}, n_{tst} \rightarrow \infty} P(\text{Sensitivity selector select Tucker or declare a tie}) \geq 1 - 2\alpha$$

If (9) holds for all $y_i = 0$, then

$$\lim_{n_{tr}, n_{ca}, n_{tst} \rightarrow \infty} P(\text{Specificity selector select Tucker or declare a tie}) \geq 1 - 2\alpha$$

Analogously, if the CP predictor $\hat{f}^{(\text{CP})}(\hat{\mathcal{C}}_i^{(\text{CP})}, \hat{\mathcal{U}}_i^{(\text{CP})})$ is consistent (i.e., satisfies the same $o_p(1)$ convergence), then the same conclusions hold for the sensitivity and specificity selectors applied to the CP structure.

7 Numerical Experiments

Data generation. The data generation process (DGP) follows the core-refinement formulation in (1) and the DC-TNN architecture in (3), specialized to a tensor covariate $\mathcal{X} \in \mathbb{R}^{D_1 \times D_2 \times D_3}$ with a binary response $y \in \{0, 1\}$. In all experiments we set $(D_1, D_2, D_3) = (32, 32, 32)$ and generate $n = 2000$ observations with $n_0 = 1000$ samples labeled 0 and $n_1 = 1000$ samples labeled 1.

Each tensor is generated from the decomposition $\mathcal{X} = \mathcal{S}(\mathcal{C}) + \mathcal{U}$, where the low-rank signal $\mathcal{S}(\mathcal{C})$ is determined by either the Tucker reconstruction map in (4) or the CP re-

construction map in (5). We consider two ground-truth regimes. In the Tucker regime, the signal is $\mathcal{S}(\mathcal{C}) = \mathcal{C} \times_1 \mathbf{U}_1 \times_2 \mathbf{U}_2 \times_3 \mathbf{U}_3$, where $\mathbf{U}_m \in \mathbb{R}^{32 \times 3}$ has orthonormal columns obtained by QR orthonormalization of an i.i.d. uniform matrix with entries in $[-5, 5]$; and the Tucker core $\mathcal{C} \in \mathbb{R}^{3 \times 3 \times 3}$ is generated by first sampling i.i.d. standard Gaussian entries, applying Gaussian kernel smoothing with bandwidth $\sigma = 1, 0$, and then rescaling to achieve Frobenius norm $\|\mathcal{C}\| = 5.0$. In the CP regime, the signal is $\mathcal{S}(\mathcal{C}) = \sum_{r=1}^R c_r \mathbf{a}_{r1} \circ \mathbf{a}_{r2} \circ \mathbf{a}_{r3}$ with CP rank $R = 12$, where each factor matrix $\mathbf{A}_m = [\mathbf{a}_{m1}, \dots, \mathbf{a}_{mR}]$ is initialized with orthonormal columns $\{\tilde{\mathbf{a}}_{rm}\}$ via QR and then perturbed to be non-orthogonal: $\mathbf{a}_{1m} = \tilde{\mathbf{a}}_{1m}$ and $\mathbf{a}_{rm} = (\tilde{\mathbf{a}}_{1m} + \eta \tilde{\mathbf{a}}_{rm}) / \|\mathbf{a}_{1m} + \eta \mathbf{a}_{rm}\|_2$ for $r \geq 2$, where $\eta = (\vartheta^{-2/3} - 1)^{1/2}$, $\vartheta = \delta / (r - 1)$ and $\delta = 0.1$. The CP coefficients $\mathbf{c} = (c_1, \dots, c_R)$ are generated from an AR(1)-type recursion: $c_1 \sim \mathcal{N}(0, 1)$ and $c_r = \rho c_{r-1} + \sqrt{1 - \rho^2} \varepsilon_r$ for $r \geq 2$ where $\varepsilon_r \stackrel{\text{i.i.d.}}{\sim} \mathcal{N}(0, 1)$ and $\rho = 0.7$, followed by rescaling to achieve $\|\mathbf{c}\|_2 = 8.0$; the CP “core” is represented as a super-diagonal tensor $\mathcal{C} \in \mathbb{R}^{R \times R \times R}$. The residual \mathcal{U} is decomposed as $\mathcal{U} = \mathcal{U}_S + \mathcal{U}_N$ into a sparse refinement component \mathcal{U}_S and a noise (nuisance component) \mathcal{U}_N . We first sample a fixed active set $J \subset [32] \times [32] \times [32]$ uniformly at random without replacement with $|J| = 18$. Conditional on J , we generate the nuisance term by sampling i.i.d. from $\mathcal{N}(0, \sigma_N^2)$ with $\sigma_N = 0.1$. The sparse refinement \mathcal{U}_S is supported on J and is constructed as follows: let j_1, \dots, j_{18} denote the 18 elements of J . For each $i = 1, \dots, 18$, we draw an independent sign $\xi_i \in \{+1, -1\}$, a scale $a_i \sim \text{Unif}[5.0, 8.0]$, and set $\mathcal{U}_S(j_i) = \xi_i a_i |\mathcal{S}(j_i)|$; all inactive coordinates are set to zero.

Finally, labels are generated by a ground-truth DC-TNN mapping $\pi(\mathcal{X}) = \sigma(z(\mathcal{C}, \mathcal{U}_D))$, where σ is sigmoid function, $z(\mathcal{C}, \mathcal{U}_D)$ is the scalar logit produced by a two-hidden-layer ($L = 2$) dual-channel tensor network with ReLU activations. To align with the refinement-channel input \mathcal{U}_D , we additionally construct an oracle dense refinement tensor $\mathcal{U}_D \in \mathbb{R}^{2 \times 3 \times 3}$ by first extraction nonzero entries of \mathcal{U}_S and then reshape to $\mathcal{U}_D \in \mathbb{R}^{2 \times 3 \times 3}$ such that

$2 \cdot 3 \cdot 3 = |J|$; and the ordering of indices in J is fixed once at the beginning of data generation. The class-balanced dataset is obtained by repeated candidate generation and acceptance into class buckets until both buckets are filled. The following table summarizes key statistics from the data generation process for both Tucker and CP regimes:

Table 2: Data Generation Summary Statistics

Structure	$\bar{z} y=1$	$\bar{z} y=0$	$\bar{\pi} y=1$	$\bar{\pi} y=0$
Tucker-generated dataset	2.542 _(2.176)	-2.256 _(1.938)	0.825 _(0.235)	0.189 _(0.256)
CP-generated dataset	3.048 _(2.810)	-2.724 _(2.351)	0.820 _(0.244)	0.176 _(0.225)

Note: Values shown as mean_(std)

Estimation. For each generated dataset, we fit the core-refinement DC-TNN estimator by the two-stage procedure described in Section 3, implementing either Tucker or CP decomposition to estimate the core tensors. This yields four experimental regimes: we fit Tucker-core and CP-core DC-TNNs on the Tucker-generated dataset, and we fit Tucker-core and CP-core DC-TNNs on the CP-generated dataset.

For each dataset, we split the $n = 2000$ observations into a training set, a calibration set, and a test set with fractions 0.6/0.2/0.2, yielding $n_{\text{tr}} = 1200$, $n_{\text{ca}} = 400$, and $n_{\text{tst}} = 400$. All tensor inputs are centered by the empirical mean of the training tensors, i.e., $\tilde{\mathcal{X}}_i = \mathcal{X}_i - \bar{\mathcal{X}}_{\text{tr}}$. In the Tucker-core estimation, we estimate shared loadings $\{\bar{\mathbf{U}}_m\}_{m=1}^3$ using a HOSVD initialization followed by HOOI refinement operated on the mode- m sample covariance. We intentionally overspecify the Tucker ranks and set $\bar{\mathbf{R}} = (\bar{R}_1, \bar{R}_2, \bar{R}_3) = (4, 4, 4)$, producing estimated cores $\hat{\mathcal{C}}_i = \tilde{\mathcal{X}}_i \times_1 \bar{\mathbf{U}}_1^\top \times_2 \bar{\mathbf{U}}_2^\top \times_3 \bar{\mathbf{U}}_3^\top \in \mathbb{R}^{4 \times 4 \times 4}$ for all splits. In the CP-core estimation, we estimate shared CP factors via a cPCA initialization followed by an ISO refinement operated on the mode- m sample covariance. We overspecify the CP rank to $\bar{R} = 16$, and after factor estimation we compute per-sample CP coefficients by contracting $\tilde{\mathcal{X}}_i$ with the pseudo-inverse loadings, embedding the resulting coefficient vector into a super-diagonal core $\hat{\mathcal{C}}_i$.

Given the estimated cores $\widehat{\mathcal{C}}_i$, we train a DC-TNN classifier $\widehat{\pi}(\mathcal{X}_i) = \widehat{f}(\widehat{\mathcal{C}}_i, \widehat{\mathcal{U}}_{D,i})$ as in (7) with learned sparse selector \mathcal{W}_u that produces a low-dimensional refinement representation $\widehat{\mathcal{U}}_{D,i} = \widehat{\mathcal{W}}_u \bullet \widetilde{\mathcal{X}}_i$. We set the refinement-channel shape to $(\overline{K}_1, \overline{K}_2, \overline{K}_3) = (3, 3, 3)$ with $\overline{K}_{\text{tot}} = 27$, network depth $L = 3$, and we apply ReLU activations with layer normalization in both channels. We optimize the binary cross-entropy loss plus the clipped- ℓ_1 selector penalty $\sum_{\mathcal{I}} \rho_{\lambda}((\mathcal{W}_u)_{\mathcal{I}})$ with clipping threshold $\tau = 0.05$ and penalty level $\lambda = 0.1$, and we train with the Adam optimizer using learning rate 10^{-3} , weight decay 10^{-4} , batch size 128.

Compare with other models. To benchmark the proposed core-refinement DC-TNN against tensor neural networks (TNNs) that exploit low-rank structure in alternative ways, we implement two additional TNNs that output $\widehat{\pi}(\widetilde{\mathcal{X}}_i) = \sigma(z_i)$. The first comparison model is imposing low-rank structure on weight tensors in Tensor Regression Layer (Low-rank TRL), each TRL is also followed by a ReLU activation, namely $\mathcal{H}^{(0)} = \widetilde{\mathcal{X}}_i$, and $\mathcal{H}^{(\ell+1)} = \text{ReLU}\{\text{TRL}(\mathcal{H}^{(\ell)})\}$ for $\ell = 0, \dots, L - 1$, the weight tensor is factorized within the layer using either a Tucker or CP parameterization; to reduce computation, the hidden tensor widths are allowed to decay across depth (e.g., $32 \rightarrow 16 \rightarrow 8 \rightarrow 4$), after which we vectorize the final hidden tensor and apply a single linear projection to produce the logit z_i and the probability $\widehat{\pi}(\widetilde{\mathcal{X}}_i)$. The second comparison model enforces low-rank structure across depth by stacking the hidden-layer regression weight tensors into a single “whole” tensor \mathcal{W} whose first mode indexes layers, so that each hidden layer uses the slice $\mathcal{W}^{(\ell)} = \mathcal{W}[\ell, :]$ in the same tensor regression update $\mathcal{H}^{(\ell+1)} = \text{ReLU}\{\text{TRL}(\mathcal{H}^{(\ell)})\}$ while keeping all hidden layers shape-preserving at $(32, 32, 32)$; we impose either a CP or Tucker factorization on \mathcal{W} (Depth-CP or Depth-Tucker). For the output layer (which is excluded from the stacking constraint), we use adaptive average pooling with $k = 6$, then apply a single linear projection to produce the logit z_i and the probability $\widehat{\pi}(\widetilde{\mathcal{X}}_i)$. Following the same experimental design, we fit both the Low-rank TRL network and the stacked-weight network under Tucker and CP

factorizations on both Tucker-generated and CP-generated datasets, yielding four model-data combinations for each baseline. We use identical train/calibration/test splits and the same BCE-based training to ensure fair comparison.

Table 3: Estimation Results on Tucker-Generated Data

Method	Test Acc	MSE (Test)	$\bar{\pi} y=1$ (Cal)	$\bar{\pi} y=1$ (Test)	$\bar{\pi} y=0$ (Cal)	$\bar{\pi} y=0$ (Test)
DC-TNN (Tucker)	0.853	0.040	0.699 _(0.215)	0.734 _(0.167)	0.321 _(0.259)	0.292 _(0.231)
DC-TNN (CP)	0.825	0.066	0.680 _(0.225)	0.705 _(0.204)	0.341 _(0.235)	0.331 _(0.226)
Stacked-TNN (Tucker)	0.798	0.078	0.699 _(0.278)	0.746 _(0.231)	0.324 _(0.304)	0.312 _(0.290)
Stacked-TNN (CP)	0.780	0.083	0.692 _(0.266)	0.720 _(0.241)	0.317 _(0.292)	0.332 _(0.283)
TRL-TNN (Tucker)	0.788	0.093	0.708 _(0.243)	0.697 _(0.246)	0.351 _(0.275)	0.337 _(0.262)
TRL-TNN (CP)	0.805	0.082	0.697 _(0.263)	0.720 _(0.245)	0.326 _(0.274)	0.319 _(0.270)

Table 4: Estimation Results on CP-Generated Data

Method	Test Acc	MSE (Test)	$\bar{\pi} y=1$ (Cal)	$\bar{\pi} y=1$ (Test)	$\bar{\pi} y=0$ (Cal)	$\bar{\pi} y=0$ (Test)
DC-TNN (CP)	0.855	0.024	0.800 _(0.266)	0.784 _(0.266)	0.223 _(0.227)	0.222 _(0.212)
DC-TNN (Tucker)	0.805	0.058	0.671 _(0.195)	0.666 _(0.196)	0.306 _(0.161)	0.330 _(0.184)
Stacked-TNN (CP)	0.728	0.117	0.671 _(0.310)	0.670 _(0.326)	0.338 _(0.316)	0.324 _(0.292)
Stacked-TNN (Tucker)	0.715	0.133	0.733 _(0.351)	0.633 _(0.389)	0.243 _(0.328)	0.250 _(0.330)
TRL-TNN (CP)	0.730	0.110	0.689 _(0.302)	0.671 _(0.319)	0.334 _(0.264)	0.338 _(0.266)
TRL-TNN (Tucker)	0.780	0.081	0.733 _(0.281)	0.706 _(0.296)	0.278 _(0.279)	0.285 _(0.273)

Uncertainty Quantification. We quantify predictive uncertainty using the conformal prediction ROC band procedure in Section 5. For each fitted model, we employ $K_{\text{tr}} = 50$ neighbors for KNN regression to approximate $\pi(\cdot)$ using predicted probabilities from the training split and $K_{\text{ca}} = 10$ nearest calibration points for local calibration sets. With miscoverage level $\alpha = 0.1$, we construct class-conditional ROC bands and AUC confidence intervals over $G = 200$ thresholds. Figures 1 and 2 display the ROC bands for DC-TNN methods on Tucker-generated and CP-generated data respectively. Tables 5 and 6 report AUC point estimates and 90% confidence intervals for all six methods on both data generation regimes, validating the coverage guarantees of Proposition 7 and Corollary 8.

Structure Selection. We evaluate the conformal ROC-based structure selector in Section 6 by comparing Tucker-core and CP-core DC-TNNs on both data generation regimes.

We define the difference score $d(\mathcal{X}) = \hat{\pi}^{\text{Tucker}}(\mathcal{X}) - \hat{\pi}^{\text{CP}}(\mathcal{X}) \in [-1, 1]$ and construct

Table 5: AUC Point Estimates and 90% Conformal Confidence Intervals on Tucker-Generated Data

Method	AUC (Sens)	CI (Sens)	AUC (Spec)	CI (Spec)
DC-TNN (Tucker)	0.838	[0.768, 0.882]	0.843	[0.805, 0.878]
DC-TNN (CP)	0.718	[0.693, 0.801]	0.723	[0.713, 0.762]
Stacked-TNN (Tucker)	0.829	[0.727, 0.905]	0.834	[0.753, 0.917]
Stacked-TNN (CP)	0.806	[0.684, 0.927]	0.805	[0.736, 0.911]
TRL-TNN (Tucker)	0.795	[0.682, 0.894]	0.800	[0.695, 0.899]
TRL-TNN (CP)	0.786	[0.689, 0.922]	0.791	[0.702, 0.897]

Table 6: AUC Point Estimates and 90% Conformal Confidence Intervals on CP-Generated Data

Method	AUC (Sens)	CI (Sens)	AUC (Spec)	CI (Spec)
DC-TNN (CP)	0.921	[0.788, 0.941]	0.925	[0.791, 0.944]
DC-TNN (Tucker)	0.858	[0.732, 0.927]	0.864	[0.751, 0.941]
Stacked-TNN (CP)	0.759	[0.559, 0.931]	0.764	[0.553, 0.931]
Stacked-TNN (Tucker)	0.758	[0.523, 0.906]	0.763	[0.522, 0.920]
TRL-TNN (CP)	0.764	[0.539, 0.910]	0.768	[0.571, 0.902]
TRL-TNN (Tucker)	0.843	[0.645, 0.919]	0.848	[0.623, 0.931]

class-conditional local calibration neighborhoods of size $K = 8$ using the weighted core-refinement distance with $w = 10$. Since each model produces its own latent representation, we compute distances in the Tucker latent space, which aligns with the null hypothesis that Tucker provides the better structure. Following Algorithm 2, we form prediction intervals at level $\alpha = 0.1$ and aggregate them into difference-ROC bands over $G = 200$ threshold values. We compute sensitivity-based and specificity-based AUC confidence intervals and apply the decision rule from Section 6.2. Figures 3 and 4 display the difference ROC bands, and Table 7 reports the selection decisions. The results validate the coverage guarantees of Theorem 9 and demonstrate the consistency property of Theorem 10, with both methods correctly identifying the true underlying structure in their respective regimes.

Table 7: Structure Selection Results via Difference ROC

Data	AUC _{Sens} [90% CI]	AUC _{Spec} [90% CI]	Decision
Tucker-generated dataset	0.785 [0.692, 0.831]	0.790 [0.723, 0.864]	DC-TNN (Tucker)
CP-generated dataset	0.149 [0.040, 0.269]	0.149 [0.047, 0.329]	DC-TNN (CP)

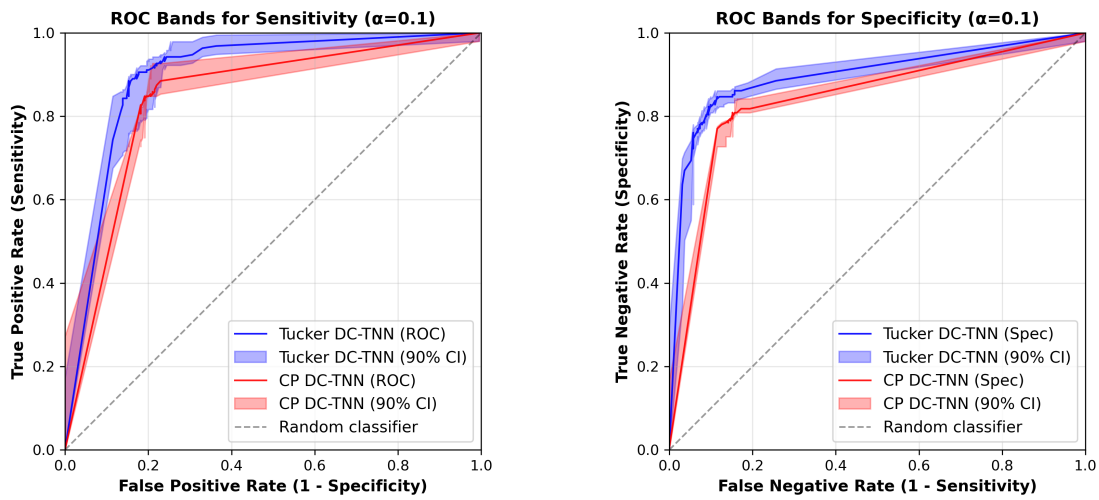


Figure 1: ROC bands with 90% conformal confidence intervals for Tucker-generated data.

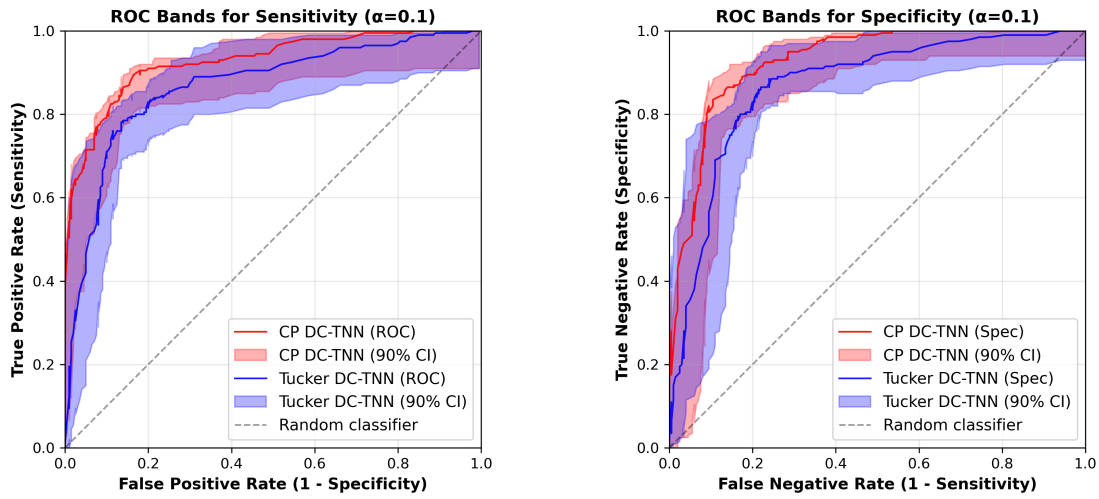


Figure 2: ROC bands with 90% conformal confidence intervals for CP-generated data.

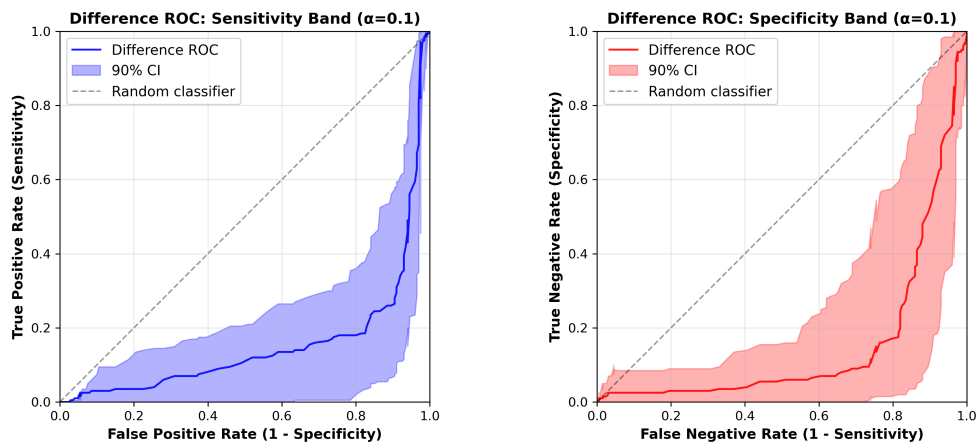


Figure 4: Difference ROC bands with 90% conformal confidence intervals for CP-generated data.

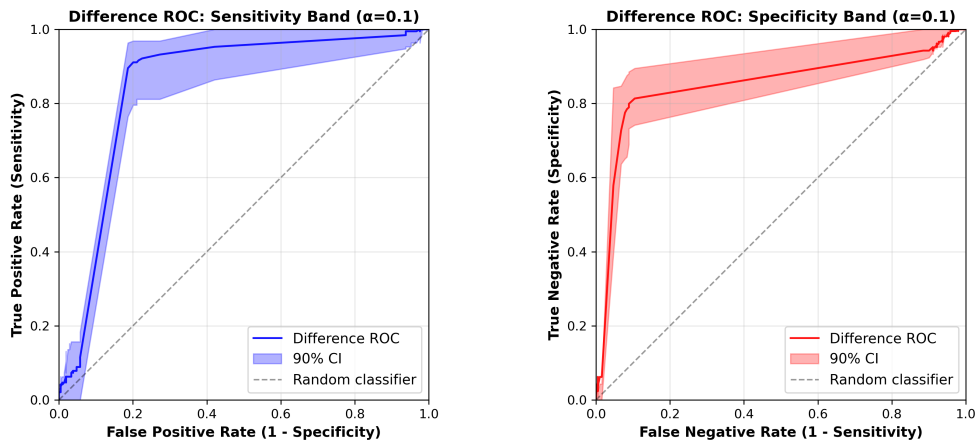


Figure 3: Difference ROC bands with 90% conformal confidence intervals for Tucker-generated data.

8 Real Data Analysis

We apply the proposed framework to the DD benchmark from TUDataset, a collection of graphs representing protein structures, where each observation is a graph G with a binary label $y \in \{0, 1\}$ indicating enzyme or non-enzyme status. Our analysis pursues two objectives: (i) benchmarking the core-refinement DC-TNN against alternative low-rank tensor neural networks, and (ii) selecting between Tucker-type and CP-type low-rank structure in a data-driven, statistically valid way.

Since the proposed methods operate on tensor covariates, we first map each graph to a fixed-dimensional tensor feature. Let $\text{PI}(G)$ denote the persistence image representation of G (construction details are deferred to the Appendix). An encoder $(G, \text{PI}(G)) \mapsto \mathcal{X} \in \mathbb{R}^{D_1 \times D_2 \times D_3}$ produces the tensor feature via two branches: a graph branch aggregating node and edge information, and a PI branch extracting multiscale topological signals, followed by a fusion module. The same encoder architecture and hyperparameters are used for all competing methods to ensure fair comparison; full details appear in the Appendix.

Implementation. We follow the same stratified train/calibration/test split strategy as in Section 7, denoting the resulting index sets by \mathcal{I}_{tr} , \mathcal{I}_{ca} , and \mathcal{I}_{te} . For each method, the

Table 8: Estimation results on the DD dataset. Values reported as mean (std).

Method	Test Acc	$\bar{\pi} y=1$ (Cal)	$\bar{\pi} y=1$ (Test)	$\bar{\pi} y=0$ (Cal)	$\bar{\pi} y=0$ (Test)
DC-TNN (Tucker)	0.803	0.638 (0.281)	0.618 (0.256)	0.265 (0.160)	0.270 (0.174)
DC-TNN (CP)	0.829	0.674 (0.263)	0.670 (0.272)	0.208 (0.202)	0.243 (0.196)
Stacked-TNN (Tucker)	0.761	0.705 (0.269)	0.752 (0.224)	0.333 (0.287)	0.333 (0.270)
Stacked-TNN (CP)	0.761	0.504 (0.325)	0.523 (0.334)	0.156 (0.171)	0.162 (0.166)
TRL-TNN (Tucker)	0.786	0.654 (0.309)	0.661 (0.299)	0.236 (0.264)	0.275 (0.267)
TRL-TNN (CP)	0.769	0.583 (0.310)	0.601 (0.193)	0.239 (0.195)	0.340 (0.210)

encoder and the downstream tensor network classifier are trained *jointly* end-to-end. To ensure fair comparison, all competing methods share the same encoder *architecture* but are each initialized from scratch with their own encoder instance.

We compare two DC-TNN variants against the TRL-TNN and Stacked-weight TNN baselines introduced in Section 7. In the Tucker-core and CP-core DC-TNN, the encoder output \mathcal{X} is further decomposed into a low-rank core $\hat{\mathcal{C}}$ via the respective factorization, and the dual-channel architecture processes $(\hat{\mathcal{C}}, \mathcal{X})$ jointly. The TRL-TNN and Stacked-weight TNN baselines map \mathcal{X} directly to the predicted probability through their respective single-channel architectures. All models are trained under the same optimization scheme and stopping rule, and we report test accuracy together with summary statistics of predicted probabilities on both the calibration and test splits.

Uncertainty Quantification. We quantify predictive uncertainty using the conformal ROC band procedure from Section 5. For each fitted model, we construct class-conditional ROC bands at miscoverage level $\alpha = 0.1$ via KNN regression to approximate $\pi(\cdot)$ on the training split and local calibration sets formed from the calibration split. Figure 5 displays the resulting sensitivity and specificity ROC bands for the DC-TNN methods, and Table 9 reports AUC point estimates with conformal confidence intervals for all methods.

Structure Selection. We apply the conformal ROC-based structure selector from Section 6 to determine which low-rank form is more strongly supported by the DD data. Since the DC-TNN explicitly decomposes each tensor covariate \mathcal{X} into a low-rank core $\hat{\mathcal{C}}$ and

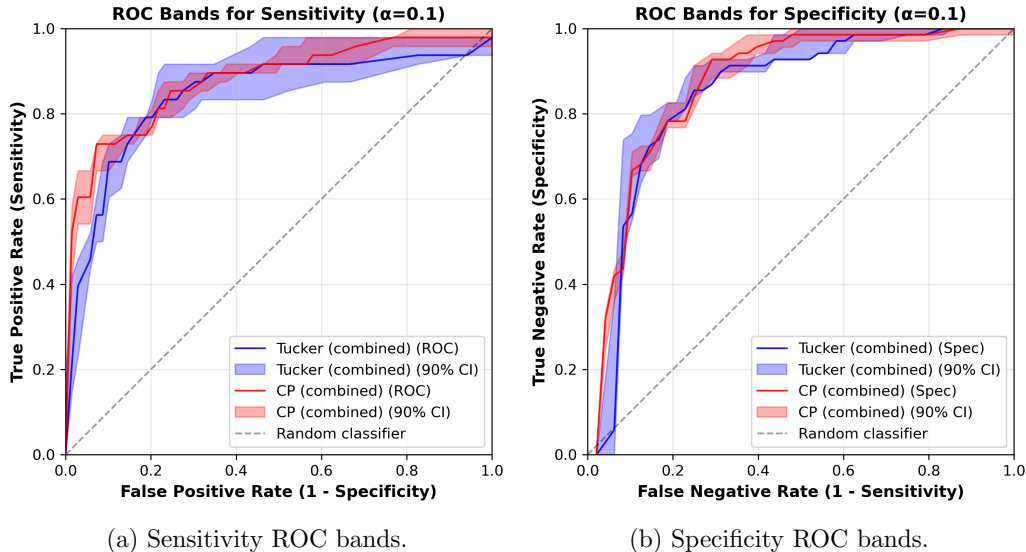


Figure 5: ROC bands with 90% conformal confidence intervals for DC-TNN methods on the DD dataset ($\alpha = 0.1$).

Table 9: AUC point estimates and 90% conformal confidence intervals on the DD dataset.

Method	AUC (Sens)	CI (Sens)	AUC (Spec)	CI (Spec)
DC-TNN (Tucker)	0.838	[0.785, 0.893]	0.836	[0.823, 0.885]
DC-TNN (CP)	0.870	[0.845, 0.899]	0.868	[0.847, 0.893]
Stacked-TNN (Tucker)	0.817	[0.743, 0.842]	0.822	[0.795, 0.884]
Stacked-TNN (CP)	0.805	[0.541, 0.833]	0.818	[0.792, 0.884]
TRL-TNN (Tucker)	0.813	[0.731, 0.863]	0.819	[0.787, 0.867]
TRL-TNN (CP)	0.781	[0.714, 0.803]	0.790	[0.682, 0.868]

a sparse refinement $\hat{\mathcal{U}}$, the structure selection is carried out exclusively for the DC-TNN variants and is framed as a two-directional conformal hypothesis test. Structure selection results for the competing model, TRL-TNN and Stacked-TNN, are reported in Appendix A.

We first test whether the Tucker factor yields better predictions than CP. The null hypothesis is $H_0^{(1)} : \hat{\pi}^{(Tucker)}$ outperforms $\hat{\pi}^{(CP)}$ against $H_a^{(1)} : \hat{\pi}^{(Tucker)}$ no better than $\hat{\pi}^{(CP)}$. Specifically, we compute the difference score $d^{(1)}(\mathcal{X}) = \hat{\pi}_{Tucker}(\mathcal{X}) - \hat{\pi}_{CP}(\mathcal{X}) \in [-1, 1]$, construct local neighborhoods using the core-refinement distance d_{FA} in (8), which measures similarity jointly in the latent core space $\hat{\mathcal{C}}^{Tucker}$ and the sparse refinement space $\hat{\mathcal{U}}^{Tucker}$, and form conformal difference ROC bands at miscoverage level $\alpha = 0.1$. To guard against directional bias, we additionally test the complementary null $H_0^{(2)} : \hat{\pi}^{(CP)}$ outperforms $\hat{\pi}^{(Tucker)}$

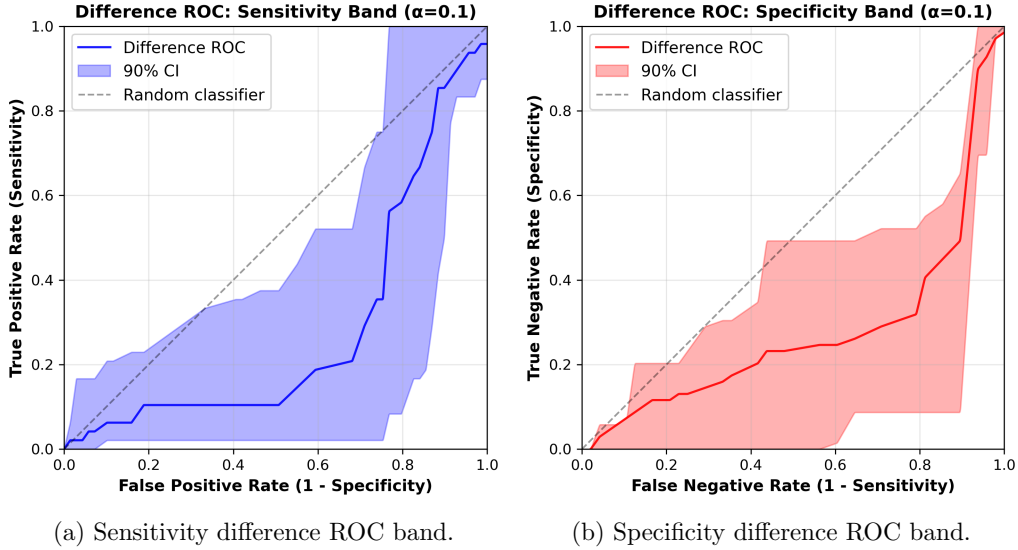


Figure 6: Test 1 ($H_0^{(1)}$): Difference ROC bands with 90% conformal confidence intervals for $d^{(1)}(\mathcal{X}) = \hat{\pi}_{\text{Tucker}}(\mathcal{X}) - \hat{\pi}_{\text{CP}}(\mathcal{X})$ on the DD dataset ($\alpha = 0.1$).

by reversing the difference score to $d^{(2)}(\mathcal{X}) = \hat{\pi}_{\text{CP}}(\mathcal{X}) - \hat{\pi}_{\text{Tucker}}(\mathcal{X})$, and changing to the CP latent space for local neighborhoods. Table 10 reports the results. Since $H_0^{(1)}$ is rejected (both AUC CIs lie entirely below 0.5) while $H_0^{(2)}$ yields a tie (CIs straddle 0.5), we conclude that Tucker does not outperform CP but CP may outperform Tucker. Those two consistent tests leads to the final selection of DC-TNN (CP). Figure 6 and Figure 7 display the corresponding difference ROC bands for $H_0^{(1)}$ and $H_0^{(2)}$, respectively.

Table 10: Structure selection results on the DD dataset via conformal difference ROC.

Test (Null H_0)	AUC _{sens} [90% CI]	AUC _{spec} [90% CI]	Decision
$H_0^{(1)} : \hat{\pi}^{(\text{Tucker})}$ outperforms $\hat{\pi}^{(\text{CP})}$	0.270 [0.121, 0.495]	0.271 [0.068, 0.421]	Reject \Rightarrow CP
$H_0^{(2)} : \hat{\pi}^{(\text{CP})}$ outperforms $\hat{\pi}^{(\text{Tucker})}$	0.694 [0.453, 0.856]	0.704 [0.558, 0.895]	Tie
Final decision: DC-TNN (CP)			

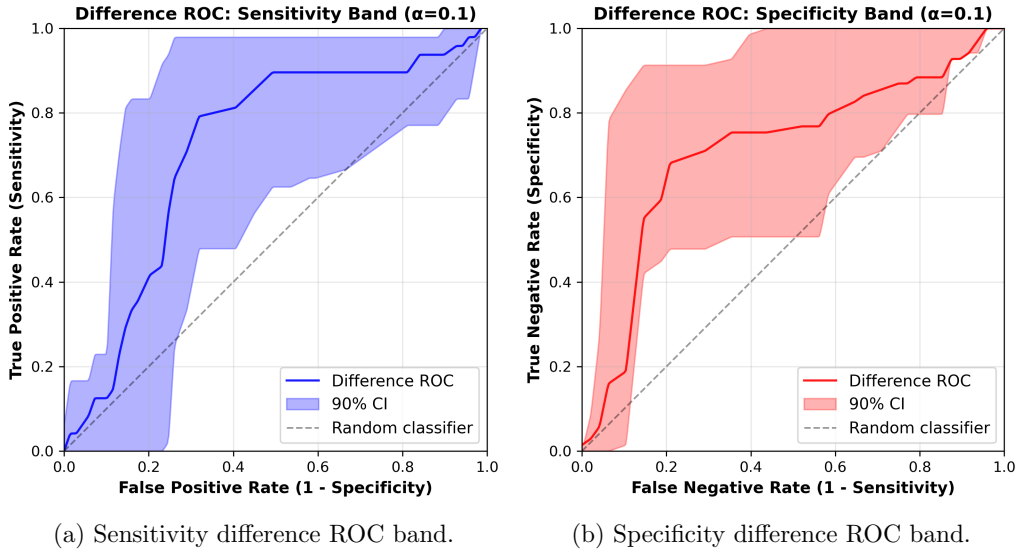


Figure 7: Test 2 ($H_0^{(2)}$): Difference ROC bands with 90% conformal confidence intervals for $d^{(2)}(\mathcal{X}) = \hat{\pi}_{\text{CP}}(\mathcal{X}) - \hat{\pi}_{\text{Tucker}}(\mathcal{X})$ on the DD dataset ($\alpha = 0.1$).

9 Conclusion

We developed a unified framework for tensor regression in which a single core-refinement representation supports estimation, distribution-free inference, and structure selection. The Dual-Channel Tensor Neural Network decomposes each tensor input into a low-rank latent core and a sparse refinement, processes them through coupled neural channels, and accommodates Tucker, CP, and tensor-train cores within a common architecture. We established non-asymptotic risk bounds whose effective dimension depends on the core rank and refinement sparsity rather than the ambient tensor size, developed structure-aware conformal ROC and AUC bands that calibrate locally in the latent space with finite-sample coverage, and introduced what is, to our knowledge, the first distribution-free procedure with finite-sample validity for selecting among candidate low-rank tensor decompositions.

Several extensions are natural. The conformal selector generalizes to more than two candidate structures via simultaneous difference-ROC bands; a global theory for end-to-end

joint estimation would complement the two-stage analysis developed here; and structure-aware calibration should extend to settings with covariate shift or temporal dependence, where ambient-space conformal methods are particularly conservative. More broadly, the results suggest that core-augmented inference may serve as a general organizing principle for statistical learning on tensor-valued data.

References

- Ahmed, T., Raja, H. & Bajwa, W. U. (2020), ‘Tensor regression using low-rank and sparse Tucker decompositions’, *SIAM Journal on Mathematics of Data Science* **2**(4), 944–966.
- Anandkumar, A., Ge, R. & Janzamin, M. (2015), ‘Guaranteed non-orthogonal tensor decomposition via alternating rank-1 updates’.
URL: <https://arxiv.org/abs/1402.5180>
- Bauer, B. & Kohler, M. (2019), ‘On deep learning as a remedy for the curse of dimensionality in nonparametric regression’, *Annals of Statistics* **47**(4), 2261–2285.
- Cai, J.-F., Li, J. & Xia, D. (2023), ‘Generalized low-rank plus sparse tensor estimation by fast Riemannian optimization’, *Journal of the American Statistical Association* **118**(544), 2588–2604.
- Chen, B., Chen, E. Y., Bolivar, S. & Chen, R. (2024), ‘Time-varying matrix factor models’, *arXiv preprint arXiv:2404.01546* .
- Chen, E., Han, Y. & Li, J. (2024a), ‘High-dimensional tensor classification with CP low-rank discriminant structure’, *arXiv preprint arXiv:2409.14397* .
- Chen, E., Han, Y. & Li, J. (2024b), ‘High-dimensional tensor discriminant analysis with incomplete tensors’, *arXiv preprint arXiv:2410.14783* .
- Chen, E., Han, Y. & Li, J. (2025), ‘High-dimensional tensor discriminant analysis: Low-rank discriminant structure, representation synergy, and theoretical guarantees’, *arXiv preprint arXiv:2512.12122* .
- Chen, E., Han, Y., Li, J. & Xu, K. (2025), ‘Modewise additive factor model for matrix time series’, *arXiv preprint arXiv:2512.25025* .
- Chen, E. Y. & Chen, R. (2022), ‘Modeling dynamic transport network with matrix factor models: with an application to international trade flow’, *Journal of Data Science* **21**(3), 490–507.

- Chen, E. Y. & Fan, J. (2023), ‘Statistical inference for high-dimensional matrix-variate factor models’, *Journal of the American Statistical Association* **118**(542), 1038–1055.
- Chen, E. Y., Fan, J. & Zhu, X. (2026), ‘Factor augmented matrix regression’, *Journal of the American Statistical Association* pp. 1–14. Published online December 2025.
- Chen, E. Y., Tsay, R. S. & Chen, R. (2020), ‘Constrained factor models for high-dimensional matrix-variate time series’, *Journal of the American Statistical Association* **115**(530), 775–793.
- Chen, E. Y., Xia, D., Cai, C. & Fan, J. (2024), ‘Semi-parametric tensor factor analysis by iteratively projected singular value decomposition’, *Journal of the Royal Statistical Society Series B: Statistical Methodology* **86**(3), 793–823.
- Chen, E. Y., Yun, X., Chen, R. & Yao, Q. (2020), ‘Modeling multivariate spatial-temporal data with latent low-dimensional dynamics’, *arXiv preprint arXiv:2002.01305* .
- DeLong, E. R., DeLong, D. M. & Clarke-Pearson, D. L. (1988), ‘Comparing the areas under two or more correlated receiver operating characteristic curves: A nonparametric approach’, *Biometrics* **44**(3), 837–845.
- Everson, R. M. & Fieldsend, J. E. (2006), ‘Multi-class ROC analysis from a multi-objective optimisation perspective’, *Pattern Recognition Letters* **27**(8), 918–927.
- Fan, J. & Gu, Y. (2023), ‘Factor augmented sparse throughput deep ReLU neural networks for high dimensional regression’, *Journal of the American Statistical Association* **0**(0), 1–15.
- Fawcett, T. (2006), ‘An introduction to ROC analysis’, *Pattern Recognition Letters* **27**(8), 861–874.
- Guan, L. (2023), ‘Localized conformal prediction: A generalized inference framework for conformal prediction’, *Biometrika* **110**(1), 33–50.
- Guhaniyogi, R., Qamar, S. & Dunson, D. B. (2017), ‘Bayesian tensor regression’, *Journal of Machine Learning Research* **18**, 1–31. Paper No. 79.
- Györfi, L. & Walk, H. (2019), Nearest neighbor based conformal prediction, in ‘Annales de l’ISUP’, Vol. 63, pp. 173–190.
- Han, R., Willett, R. & Zhang, A. R. (2022), ‘An optimal statistical and computational framework for generalized tensor estimation’, *Annals of Statistics* **50**(1), 1–29.
- Hao, B., Zhang, A. R. & Cheng, G. (2020), ‘Sparse and low-rank tensor estimation via cubic sketchings’, *IEEE Transactions on Information Theory* **66**(9), 5927–5964.

- He, L., Chen, K., Xu, W., Zhou, J. & Wang, F. (2018), Boosted sparse and low-rank tensor regression, *in* ‘Advances in Neural Information Processing Systems 31 (NeurIPS)’.
- Kohler, M. & Langer, S. (2021), ‘On the rate of convergence of fully connected deep neural network regression estimates’, *The Annals of Statistics* **49**(4), 2231–2249.
- Kong, L., Chen, E., Chen, Y. & Han, Y. (2025), TEAFormers: Tensor-augmented transformers for multi-dimensional time series forecasting, *in* ‘IJCAI 2025 AI for Time Series Workshop’. arXiv:2410.20439.
- Kossaifi, J., Lipton, Z. C., Kolbeinsson, A., Khanna, A., Furlanello, T. & Anandkumar, A. (2020), ‘Tensor regression networks’, *Journal of Machine Learning Research* **21**(123), 1–21.
- Lei, J., G’Sell, M., Rinaldo, A., Tibshirani, R. J. & Wasserman, L. (2018), ‘Distribution-free predictive inference for regression’, *Journal of the American Statistical Association* **113**(523), 1094–1111.
- Li, L. & Zhang, X. (2017), ‘Parsimonious tensor response regression’, *Journal of the American Statistical Association* **112**(519), 1131–1146.
- Li, X., Xu, D., Zhou, H. & Li, L. (2018), ‘Tucker tensor regression and neuroimaging analysis’, *Statistics in Biosciences* **10**(3), 520–545.
- Liu, L., Chen, E., Han, Y. & Xia, L. (2025), ‘Tensor Neyman-Pearson classification: Theory, algorithms, and error control’, *arXiv preprint arXiv:2512.04583*.
- Liu, X. & Chen, E. Y. (2019), ‘Helping effects against curse of dimensionality in threshold factor models for matrix time series’, *arXiv preprint arXiv:1904.07383*.
- Liu, X. & Chen, E. Y. (2022), ‘Identification and estimation of threshold matrix-variate factor models’, *Scandinavian Journal of Statistics* **49**(3), 1383–1417.
- Lock, E. F. (2018), ‘Tensor-on-tensor regression’, *Journal of Computational and Graphical Statistics* **27**(3), 638–647.
- Majnik, M. & Bosnić, Z. (2013), ‘ROC analysis of classifiers in machine learning: A survey’, *Intelligent Data Analysis* **17**(3), 531–558.
- Nakas, C. T., Bantis, L. E. & Gatsonis, C. A. (2023), *ROC Analysis for Classification and Prediction in Practice*, Chapman and Hall/CRC.
- Novikov, A., Podoprikin, D., Osokin, A. & Vetrov, D. P. (2015), Tensorizing neural networks, *in* ‘Advances in Neural Information Processing Systems 28 (NeurIPS)’, pp. 442–450.

- Oseledets, I. V. (2011), ‘Tensor-train decomposition’, *SIAM Journal on Scientific Computing* **33**(5), 2295–2317.
- Raskutti, G., Yuan, M. & Chen, H. (2019), ‘Convex regularization for high-dimensional multiresponse tensor regression’, *Annals of Statistics* **47**(3), 1554–1584.
- Romano, Y., Patterson, E. & Candès, E. J. (2019), Conformalized quantile regression, in ‘Advances in Neural Information Processing Systems 32 (NeurIPS)’.
- Schmidt-Hieber, J. (2020), ‘Nonparametric regression using deep neural networks with ReLU activation function’, *Annals of Statistics* **48**(4), 1875–1897.
- Shafer, G. & Vovk, V. (2008), ‘A tutorial on conformal prediction’, *Journal of Machine Learning Research* **9**(3).
- Si, Y., Zhang, Y. & Li, G. (2022), ‘An efficient tensor regression for high-dimensional data’, *arXiv preprint arXiv:2205.13734*.
- Sun, W. W., Lu, J., Liu, H. & Cheng, G. (2017), ‘Provable sparse tensor decomposition’, *Journal of the Royal Statistical Society, Series B* **79**(3), 899–916.
- Venkatraman, E. S. & Begg, C. B. (1996), ‘A distribution-free procedure for comparing receiver operating characteristic curves from a paired experiment’, *Biometrika* **83**(4), 835–848.
- Vovk, V., Gammerman, A. & Shafer, G. (2005), *Algorithmic Learning in a Random World*, Springer.
- Wen, T., Chen, E. & Chen, Y. (2024), Tensor-view topological graph neural network, in ‘Proceedings of the 27th International Conference on Artificial Intelligence and Statistics (AISTATS)’, Vol. 238 of *Proceedings of Machine Learning Research*, PMLR, Valencia, Spain, pp. 4330–4338.
- Wen, T., Chen, E., Chen, Y. & Lei, Q. (2025), Bridging domain adaptation and graph neural networks: A tensor-based framework for effective label propagation, in ‘Conference on Parsimony and Learning (CPAL)’.
- Wu, Y., Mo, J., Chen, E. & Chen, Y. (2025), Tensor-fused multi-view graph contrastive learning, in ‘Advances in Knowledge Discovery and Data Mining (PAKDD)’, Vol. 15876 of *Lecture Notes in Computer Science*, Springer Nature Singapore, pp. 16–28.
- Wu, Y., Yang, B., Chen, E., Chen, Y. & Zheng, Z. (2025), Conditional prediction ROC bands for graph classification, in ‘Proceedings of the 28th International Conference on Artificial Intelligence and Statistics (AISTATS)’, Vol. 258 of *Proceedings of Machine Learning Research*, PMLR, pp. 2458–2466.

- Wu, Y., Yang, B., Zhao, Y., Chen, E., Chen, Y. & Zheng, Z. (2024), ‘Conditional uncertainty quantification for tensorized topological neural networks’, *arXiv preprint arXiv:2410.15241* .
- Xu, K., Chen, E. & Han, Y. (2025), ‘Statistical inference for low-rank tensor models’, *arXiv preprint arXiv:2501.16223* .
- Zhang, A. & Xia, D. (2018), ‘Tensor SVD: Statistical and computational limits’, *IEEE Transactions on Information Theory* **64**(11), 7311–7338.
- Zheng, Z., Yang, B. & Song, P. (2024), ‘Quantifying uncertainty in classification performance: ROC confidence bands using conformal prediction’, *arXiv preprint arXiv:2405.12953* .
- Zheng, Z., Yang, B. & Song, P. (2025), ‘Classification uncertainty quantification: A comparison between bootstrap and conformal ROC confidence bands’, *Statistica Sinica* **37**(4). In press.
- Zhou, H., Li, L. & Zhu, H. (2013), ‘Tensor regression with applications in neuroimaging data analysis’, *Journal of the American Statistical Association* **108**(502), 540–552.